INFORMATION TO USERS

This manuscript has been reproduced from the microfilm master. UMI films the text directly from the original or copy submitted. Thus, some thesis and dissertation copies are in typewriter face, while others may be from any type of computer printer.

The quality of this reproduction is dependent upon the quality of the copy submitted. Broken or indistinct print, colored or poor quality illustrations and photographs, print bleedthrough, substandard margins, and improper alignment can adversely affect reproduction.

In the unlikely event that the author did not send UMI a complete manuscript and there are missing pages, these will be noted. Also, if unauthorized copyright material had to be removed, a note will indicate the deletion.

Oversize materials (e.g., maps, drawings, charts) are reproduced by sectioning the original, beginning at the upper left-hand corner and continuing from left to right in equal sections with small overlaps. Each original is also photographed in one exposure and is included in reduced form at the back of the book.

Photographs included in the original manuscript have been reproduced xerographically in this copy. Higher quality 6" x 9" black and white photographic prints are available for any photographs or illustrations appearing in this copy for an additional charge. Contact UMI directly to order.

U·M·I

University Microfilms International
A Bell & Howell Information Company
300 North Zeeb Road, Ann Arbor, MI 48106-1346 USA
313/761-4700 800/521-0600

Order Number 9319573

Microcalorimetry of the adsorption of lysozyme onto uncharged substrates

Lee, Valerie A., Ph.D.

The University of Michigan, 1993

U·M·I
300 N. Zeeb Rd.
Ann Arbor, MI 48106

MICROCALORIMETRY OF THE ADSORPTION OF LYSOZYME ONTO UNCHARGED SUBSTRATES

by

Valerie A. Lee

A dissertation submitted in partial fulfillment
of the requirements for the degree of
Doctor of Philosophy
(Biomaterials and
Materials Science and Engineering)
in The University of Michigan
1993

Doctoral Committee:

Professor Robert G. Craig, Co-Chair
Professor Frank E. Filisko, Co-Chair
Professor William J. O'Brien
Professor Richard E. Robertson
Professor Robert Zand

RULES REGARDING THE USE OF

MICROFILMED DISSERTATIONS

Microfilmed or bound copies of doctoral dissertations submitted to The University of Michigan and made available through University Microfilms International or The University of Michigan are open for inspection, but they are to be used only with due regard for the rights of the author. Extensive copying of the dissertation or publication of material in excess of standard copyright limits, whether or not the dissertation has been copyrighted, must have been approved by the author as well as by the Dean of the Graduate School. Proper credit must be given to the author if any material from the dissertation is used in subsequent written or published work.

ACKNOWLEDGMENTS

Thanks are given to each of my committee members for their assistance with this work. Thanks are also given to Dr. John Halloran, Dr. David Srolovitz, Dr. Stacy Bike and Dr. Fred Terry for helpful discussions.

TABLE OF CONTENTS

ACKNOWLEDGEMENTS ii

LIST OF FIGURES v

LIST OF TABLES vii

LIST OF APPENDICES viii

CHAPTER

I. INTRODUCTION 1

II. REVIEW OF LITERATURE 6

III. MATERIALS AND METHODS 12

Buffer Preparation 12
Purification of Lysozyme 13
Lysozyme Water Content 14
Gel Electrophoresis 14
Polymer Sample Preparation 15
Verification of Adsorption 17
Determination of Surface Area 17
Adsorption Isotherm 18
Minimum Polystyrene Thickness Required to Mask Silicon Oxide Properties 18
TEM Study of High-Surface Area Sample 19
Wilhelmy Plate 20
Pendant Drop 22
Polymer Densities 24
Microcalorimetry 26
Preparation of Lysozyme Solutions 32
Amount of Lysozyme Adsorbed by Substrate 32
Infrared Study of Conformational Changes 33

IV. RESULTS AND DISCUSSION 35

Protein Preparation 35
Sample Preparation 37
Interfacial Energies 44
Wilhelmy Plate 53
Microcalorimetry 59

V. SUMMARY 80

VI. CONCLUSIONS 84

APPENDICES 85

BIBLIOGRAPHY 96

LIST OF FIGURES

Figure

1. Wilhelmy hysteresis loop. 21

2. Cross-sectional sketch of pendant drop apparatus. 23

3. Cross-sectional sketch of Tian-Calvet microcalorimeter. 26

4. Two-tube reaction cell assembly. 30

5. Fractions obtained by chromatography of lysozyme on Bio-Rex 70 at 25°C and pH of 7.14. 36

6. SDS-PAGE gel electrophoresis of lysozyme fractions 3, 4 and 5. 37

7. Determination of water content of lyophilized lysozyme. 38

8. Infrared spectra: a. Silica, as-received, and b. Silica, heat-treated at 900°C for 10 minutes in vacuum. 39

9. Infrared spectra showing progress of adsorption of polystyrene by silica in carbon tetrachloride. 40

10. Adsorption isotherms of sample polymers on silica. 41

11. Electron micrographs:
    a. Uncoated silica
    b. Polystyrene-coated silica. 43

12. Contact angles vs thickness of polystyrene layer. 44

13. Surface tensions of polymers as a function of temperature determined by pendant drop method. 48

14. Polymer densities as a function of temperature. 48

15. Wilhelmy hysteresis loop obtained from acid-cleaned, oxide-covered silicon wafer. 55

16. Contact angles vs immersion time in water from Wilhelmy plate results on thick samples. 56

17. Contact angles vs immersion time in water from Wilhelmy plate results on thin samples. 58

18. Resolution of the integral heat of adsorption of:
a. Bovine pancreas ribonuclease, and
b. Human serum albumin into its components.
Substrate - negatively charged polystyrene.
(Adapted from Norde and Lyklema, 1979). 63

19. Adsorption isotherm (▲) and microcalorimetric heats (O) for polystyrene at ionic strength of 0.1M from phosphate buffer. 65

20. Adsorption isotherm (▲) and microcalorimetric heats (O) for styrene/butyl methacrylate at ionic strength of 0.1M from phosphate buffer. 66

21. Adsorption isotherm (▲) and microcalorimetric heats (O) for styrene/allyl alcohol at ionic strength of 0.1M from phosphate buffer. 67

22. FTIR spectra of amide I and II bands:
a. Bulk lysozyme, I/II=1.36,
b. Polystyrene/lysozyme, I/II=1.42,
c. Styrene/butyl methacrylate/lysozyme, I/II=1.76, and
d. Styrene/allyl alcohol/lysozyme, I/II=2.56. 68

23. Schematic drawings of adsorption isotherm and concentration of protein remaining in solution.
I = expanded protein phase, II = condensed protein phase.
(Adapted from Levine, 1969). 71

24. Adsorption isotherm and concentration of lysozyme remaining in solution for polystyrene at ionic strenth 0.1M from phosphate buffer. 71

25. Schematic drawing of protein conformations and resulting heats assuming identical starting conditions at points A, B and C. 73

26. Adsorption isotherm (▲) and microcalorimetric heats (o) for polystyrene at ionic strength of 0.002M from phosphate buffer. 75

27. Adsorption isotherm (▲) and microcalorimetric heats (o) for styrene/butyl methacrylate at ionic strength of 0.002M from phosphate buffer. 76

28. Adsorption isotherm (▲) and microcalorimetric heats (o) for styrene/allyl alcohol at ionic strength of 0.002M from phosphate buffer. 77

LIST OF TABLES

Table

1. Surface and component energies for sample polymers from contact angles and harmonic mean approximation. 51

2. Surface and component energies for sample polymers from geometric mean approximation and pendant drop results. 52

3. Interfacial energies of polymers in water from harmonic mean equation and from geometric mean equation and pendant drop results. 52

LIST OF APPENDICES

Appendix

A. Procedure-Gel Electrophoresis 86

B. Components of Surface Energy and Interfacial Energies of Sample Polymers 89

C. Tabulated Data 90

CHAPTER I

INTRODUCTION

The success of a material chosen for use in implanted prosthetic devices depends on two factors. First, mechanical properties must be suited to the intended application. Second, the material must be compatible in an environment of biological fluids.

While implant applications require a wide range of mechanical properties, this requirement is the easier of the two to satisfy. The selected material must possess sufficient resistance to compression, tension and shear that may develop during use. Current technology permits the preparation of devices with mechanical properties suitable for nearly any biomedical application. For example, the flexibility requirements of synthetic vascular grafts and catheters can be adequately provided by various polymeric materials or by a knitted or woven fiber. In contrast, the load bearing function of the ball of a hip prosthesis requires considerable rigidity and superior wear characteristics. High density alumina is satisfactory for this purpose.

Compatibility in biological fluids, on the other hand, concerns the acceptance of the implant by the body, and is largely a response to implant surface characteristics. Implant/host interactions are complex, and have been shown to depend on surface charge[1], surface free energy[2], chemical

group distribution, surface texture, porosity[3], smoothness and flow conditions[4]. Implant-induced adverse reactions as varied as toxic, allergic and inflammatory responses have been reported. In particular, in the case of blood-contacting implants such as vascular grafts, prosthetic heart valves, external arteriovenous shunts for blood access in hemodialysis and artificial hearts, normal host protective mechanisms trigger the intrinsic coagulation system upon implant contact, and with time surface-induced thrombi are inevitable. Each of these responses poses a particular danger to the host.

Overall, biocompatibility is a difficult requirement to realize. To date, no synthetic material has emerged as an acceptable blood-contacting material for long term use.

The current approach in the development of nonthrombogenic materials aims to interrupt thrombus formation at some point in the clotting cascade. Biological fluids contain a number of diverse interacting components such as proteins, lipids, carbohydrates, salts and cellular elements in an aqueous medium. When a fluid such as blood contacts a nonphysiologic surface, the host's normal wound healing mechanism initiates a series of events. Specific proteins, consisting mainly of fibrinogen, adsorb onto the surface[5]. After the deposition of a layer of protein, platelets adsorb onto the protein-covered surface, flatten, become activated and aggregate irreversibly with other platelets from the blood. Platelet activation generally signals the onset of a number of events involving several blood components and ending in the formation of a thrombus on the surface of the solid. This sequence of events is encountered on all types of synthetic surfaces.

One way to eliminate thrombus formation is to prevent the adhesion of platelets. Platelets have been found not to adhere to heparinized surfaces[6].

The immobilization of heparin on a surface by grafting has resulted in materials suitable for use as short-term blood-contacting catheters.

The blood protein albumin is thought to contain none of the peptide sequences which interact with adhesion receptors on cell membranes or with blood factors in the clotting cascade. The passivation by albumin of surfaces which preferentially adsorb that blood protein has resulted in improved biocompatibility[6].

While the above two methods have been shown to be suitable for short-term applications, with time and for reasons not clearly understood, the formation of thrombi at the surface again becomes a problem.

Ruckenstein has proposed that the ideal long-term blood-contacting surface may be one on which no proteins adsorb[7]. He reasons that a non-adsorbing surface may not trigger the coagulation mechanism at all, and proposes that device surfaces be modified in accordance with this principle. Since it is known that extremely biocompatible interfaces, such as the cell membrane/blood plasma junction, have very low interfacial energies on the order of 1-3 ergs/cm^2[8,9], Ruckenstein suggests that the implant/blood interfacial energy may be a suitable guiding parameter.

Interfacial energy may be a relevant parameter in the following way. A nonphysiologic surface in contact with blood results in the creation of a new interface, the biomaterial/blood interface. A thermodynamic driving force is thus generated for reducing the interfacial energy at the new interface. Proteins, the most surface active component of blood, adsorb almost instantaneously. At an interface with high interfacial energy, proteins will tend to interact with the surface extensively, perhaps by anchoring at multiple sites, thereby decreasing the interfacial energy. The adsorbed

protein will undergo a substantial change in conformation relative to its native state in solution.

The new protein-covered surface exposed to the blood has lower, though still substantial, energy compared to the original interface. Adsorption of further protein layers, platelet flattening and platelet activation will tend to continue.

In contrast, if the interfacial energy is low, the thermodynamic driving force for adsorption will be small. Proteins will interact less extensively with the surface, perhaps anchoring at fewer sites. Conformational changes upon adsorption will be less pronounced, and the tendency for continued adsorption and platelet activation will be smaller.

Typical blood-contacting materials in current use are polymeric. Polymers have the ability to adopt different surface configurations in different environments so as to increase the interaction between phases and thereby decrease the interfacial energy. Polymers are generally processed under ambient conditions, but upon use in biomedical applications, encounter an aqueous environment. Ideally, the guiding parameter chosen would include characteristics of the two interacting phases at equilibrium.

The purpose of this research is to examine the relationship between the adsorption of lysozyme and the surface/water interfacial energies of three polymeric substrates. The affinity of lysozyme for each substrate, the amount of lysozyme adsorbed, and in particular, its conformational state after adsorption are studied. It is known that materials vary widely in their biocompatibilities and clotting rates. Relevant material properties must necessarily be reflected through the adsorbed protein layer as variations in protein conformation. In this way, the suitability of the substrate/water

interfacial energy as a predicting parameter for biocompatibility can be determined.

Surface energies of each substrate are measured in the molten form by the pendant drop method and extrapolated to room temperature. The work of adhesion at each substrate/water interface is estimated from contact angle measurements and assumptions regarding the nature of forces operating there. These results, along with published surface and component tensions of water, allow the estimation of the interfacial energy. This method, however, is unable to estimate changes to the interfacial energy from polymer surface restructuring.

The time-dependent nature of the substrate surface upon contact with water is verified by a Wilhelmy plate study.

Heats of adsorption of protein by each substrate, obtained using a microcalorimeter, provide insight into conformational changes occurring upon adsorption.

CHAPTER II

REVIEW OF LITERATURE

The behavior of proteins at interfaces is relevant to both natural and technical processes, and studies of their adsorption have been reported since the first part of this century. An early source of information includes the literature on fundamental surface science at the air/water interface[9]. Later major sources include the solid-liquid chromatography literature[10-11] and the literature dealing with soils and minerals[12]. Interest in protein interaction with materials used in medical devices has been considerable in the last twenty-five years or so[13-14].

From the literature, it appears that most proteins interact with most surfaces. A variety of techniques have been used to study these interactions such as spectroscopy, radio labeling, and electrochemical, optical, and thermodynamic methods. However, despite this diversity of techniques, general conclusions regarding the behavior of proteins at interfaces are difficult, primarily because of the complexity of the phenomenon.

Adsorption: With respect to structural changes in adsorbed protein, much evidence is indirect, such as a layer thickness smaller than the shortest axis of the native molecule[15], a reduction of biological activity upon adsorption[16], and the influence of temperature on the adsorption isotherm[17]. Most of the more direct methods, primarily spectroscopic, support a conformationally

changed adsorbed molecule[18-22]. Calorimetric studies of some systems have shown an endothermic heat upon initial adsorption of protein molecules[23-26]. This result suggests an entropically driven process, the entropy gain probably arising from an increased translational entropy of water and/or decreased secondary structure within the protein.

The free energy of adsorption is generally reflected in the shape of the adsorption isotherm. In the case of flexible highly solvated homopolymers with high affinity, isotherms with continuously increasing adsorbed amounts are often obtained. Polymer molecules attach to a sorbent surface via multiple contacts, forming loops and tails, and as the adsorbed amount increases, structural rearrangements within the molecules occur, resulting in a decreasing adsorbed fraction[27]. However, while compact, globular proteins such as ribonuclease may flatten and denature to some extent upon adsorption, they have intramolecular forces strong enough to maintain a rather compact shape. The occurrence of isotherms having a finite initial slope and a definite plateau are more common[28].

The occurrence of isotherms with multiple plateaus have been reported[29-32]. The plateaus have been postulated to correspond to distinct protein surface conformations.

The hydrophobicities of protein and sorbent appear to influence adsorption. It is generally found that the adsorbed amount is higher on hydrophobic than on hydrophilic surfaces[15,16,33-35]. There is also evidence that the binding affinity is higher[16,33,36], and that structural changes are more pronounced with increasing hydrophobicity of the sorbent[16,37].

The overall hydrophobicity of the protein may be relevant. It is thought that dehydration of hydrophobic parts of the substrate surface and protein contribute to entropy gain and may promote spontaneous adsorption. It was

found by Birdi[38], who examined a series of proteins at the air-water interface, that a stronger tendency to structural alteration followed increasing protein hydrophobicity. Norde, et al.[17,39-42], found structural alterations to occur upon adsorption in the relatively hydrophobic albumin molecule, while such a change was either smaller or absent in the less hydrophobic ribonuclease molecule.

Electric charge and ionic strength: With respect to the effect of electric charge, it is usually found that adsorption is at a maximum near the isoelectric point of the protein[33,43,44]. This result is the case for most proteins, including albumin, whose structural stability decreases away from the isoelectric point as a result of charging[43]. For the few proteins such as ribonuclease, whose structures are strongly stabilized by internal cohesion, no dependence of adsorption upon pH is found. This contrast is further evidenced by the ease with which albumin adsorbs on both hydrophilic and hydrophobic surfaces, whereas ribonuclease easily adsorbs on hydrophobic surfaces, but on hydrophilic surfaces only if it is electrostatically favored[28].

The presence of low molecular weight electrolytes generally screen interaction between charges, and increased adsorption is usually observed upon increasing ionic strength[17]. However, the influence of electrolyte concentration is difficult to analyze. It has been reported that the effect of the ionic strength on adsorption is dependent upon the type of substrate[44], and that adsorption is sensitive to the type of ions present[45].

Techniques for determining organization within the adsorbed layer are few. Thickness and compactness can be determined by ellipsometry. Cuypers et al.[15,46] showed that while hydrophobic surfaces adsorb much greater amounts than hydrophilic surfaces, the layer on the hydrophobic surface is much more compact. They also showed that in some systems, both hydrophilic

and hydrophobic, the initial layer was adsorbed in a loose fashion and subsequently rearranged to become compact. In the systems studied, this effect occurred within minutes.

Calorimetry: To date, only calorimetric studies have resulted in information whereby the structure at various points within the adsorbed layer can be advanced. In a series of papers, Nyilas et al.[24-26] examined the adsorption of blood proteins on glass and carbon surfaces. Their results suggest that the initially adsorbed layer undergoes more conformational changes than do subsequent layers. Filisko et al.[23] have proposed a model for the adsorbed layer where the initially adsorbed molecules are denatured and subsequent layers are successively more ordered, until at maximum thickness a highly ordered state exists.

Other calorimetric studies include those of Korn and Killman[47] for the adsorption of uncharged homopolymers on silica. All heats were exothermic and a reduced bound fraction with increasing adsorbed amount was found.

Norde et al.[39,44] systematically examined the effect of charge on the heat effect. They concluded that there is no simple relationship between the heat of adsorption and the charge on either the protein or sorbent.

Polymer surface mobility: It is now evident that polymer surface molecules exhibit motions and relaxations similar to their bulk relaxation phenomena, and are relatively mobile in comparison to metals and ceramics. These motions permit the reorientation of the polymer surface to minimize the interfacial free energy. Holly and Refojo[48] concluded from contact angle hysteresis studies of soft contact lens materials that the methacrylate backbone was exposed to the surface in air, while the hydroxylated pendant groups were oriented toward the surface in water. Sung and Hu[49] showed that the Auger spectrum of a segmented urethane-siloxane polymer is quite different for that

of the air-dried surface and the bottom surface in contact with the casting mold. Polyethylene surfaces have been shown to modify structurally due to adsorbate interaction[50]. It also appears that even rigid, hydrophobic polymers such as polystyrene[51] and poly(methyl methacrylate)[52] reorient in contact with water.

The time scale involved for environmentally induced surface relaxations range from one second or less for some types of hydrogels to hours or days for other polymers such as oxygen-plasma treated poly(propylene)[53].

Methods used to study contact angle hysteresis have included the Wilhelmy plate method, and the sessile bubble and captured air bubble techniques[48,51,54].

Interfacial energies: Fowkes[55] suggested in 1964 that the dispersion force contribution to the work of adhesion at interfaces could be approximated by the geometric mean of the dispersion force contribution of the surface tensions of the interacting phases. Since then a large literature became available which attempted to determine polar and apolar components of interfacial free energies of solids in liquids by appropriate assumptions and approximations. Some extended Fowkes' technique to the polar contributions to the interfacial free energy by assuming the geometric mean approximation applied for those interactions as well[56].

A harmonic mean approximation was developed by Wu[57] for use in low energy systems such as organic liquids, polymers and water. Wu states that a geometric-harmonic mean equation is preferred for high energy systems such as mercury, glass and metal oxides.

Correlation of biocompatibility and substrate energy parameters: Ko et al.[58] determined the individual surface free energy components of several grafted copolymers of hydroxyethyl methacrylate and ethyl

methacrylate of varying composition and water content in both the hydrated and unhydrated states. For all solid surfaces, the polar component of the surface free energy was increased and its dispersion component decreased in the hydrated state in comparison to the unhydrated state. The change in the polar component was much more pronounced than that of the dispersion component, and the solid-water interfacial free energies as calculated by Ruckenstein[7] decreased with increasing water content. The highest in vivo blood compatibility for a series of these materials was found by Ratner et al.[59] to occur at a surface water content of 15%. This observation correlates well with Ko's results where the estimated interfacial energy of a material with 17% surface water content was 0.92 ergs/cm^2, and with Ruckenstein's proposal[7] that for high biocompatibility a material must exhibit a low interfacial free energy near 1-3 ergs/cm^2.

Interfacial free energies were estimated for a series of four polymer surfaces by Brynda et al.[60] using contact angles and the geometric mean approximation. A fair correlation between interfacial free energy and the amount of adsorbed human serum albumin and fibrinogen was observed.

Baszkin and Lyman[61] estimated the polar and dispersion components of the work of adhesion for a series of relatively hydrophobic polymers and concluded that less adsorption of bovine albumin, γ-globulin and fibrinogen occurred when the polar component was large compared to the dispersion component.

From cell spreading studies on a variety of substrates, Baier[62] notes that minimal adhesion occurs for those materials whose critical surface tension is in the range of 20-30 mNm^{-1}.

CHAPTER III

MATERIALS AND METHODS

Buffer preparation

Phosphate buffer of pH 7.14 and ionic strength 0.1M was prepared from monobasic (KH_2PO_4, MW 136.09) and dibasic (K_2HPO_4, MW 174.18) potassium salts in the following way[63]:

1) $pH = pK_a + \log([salt]/[acid])$, Henderson-Hasselbach equation (1)

a) $H_2PO_4^- \xrightarrow{pKa\ 7.21} HPO_4^{2-}$, pK_a of relevant reaction (2)

2) For 1 liter of buffer (0.1 mole of phosphate):

a) $7.14 = 7.21 + \log([HPO_4^{2-}]/[H_2PO_4^-])$ (3)

b) $0.851 = [HPO_4^{2-}]/[H_2PO_4^-]$ = ratio of 0.851/1 (4)

c) $(0.851/1.851) \cdot 0.1$ mole = 0.0460 mole of HPO_4^{2-}, (5)
or 8.01 grams K_2HPO_4, and

d) $(1/1.851) \cdot 0.1$ mole = 0.0540 mole of $H_2PO_4^-$, (6)
or 7.35 grams KH_2PO_4 were needed.

These quantities were dissolved in sufficient deionized water to make 1 liter. The pH was adjusted to 7.14 by the addition of KOH.

Buffers of pH 7.14 and ionic strengths 0.002M and 0.2M were prepared in a similar way.

Purification of Lysozyme

Hen egg white lysozyme (3x crystallized, Sigma) was purified using an ion-exchange method outlined by Saxena and Wetlaufer[64]. Bio-Rex 70, 200-400 mesh (Bio-Rad), was soaked overnight in 0.2M phosphate buffer, pH 7.14, and packed in increments into a 1 x 45 inch glass column to a height of 30 inches. A nylon mesh covered end fitting with tubing was attached to the bottom of the column, through which buffer could drain. A similar stopper at the top of the column was attached to tubing from a buffer reservoir. Buffer from the reservoir was run slowly through the column for several hours to ensure complete packing. Buffer was then allowed to drain from the column until it was even with the level of the resin.

One and one-half g of lysozyme, previously dissolved in 25 ml of buffer and centrifuged to remove a large insoluble fraction, was layered using a syringe-tubing combination onto the surface of the resin. The protein solution was allowed to enter the column until it was flush with the resin. Buffer was then carefully added without disturbing the resin surface until it was within 6 inches of the top of the column. The eluate from the column was collected in test tubes contained in an automatic fraction collector that changed tubes every 15 minutes. The drip rate was set at 10 ml/15 minutes.

The above procedure was carried out at room temperature and took approximately 48 hours to complete. Filled test tubes were kept in a cold room (4°C). The above procedure was repeated 22 more times.

The collected fractions were monitored at 280 nm. Five distinct fractions were found.

Fractions 3, 4 and 5 from the first column run were collected and dialyzed separately against deionized water for two days, (two water changes), using 6000-8000 MW cutoff Spectra-Por membranes. The protein was lyophilized and stored at -15°C in a desiccator.

In subsequent column runs, fractions 3, 4 and 5 were collected, dialyzed, and lyophilized as one. A total of about 12 grams of purified protein was obtained, for a yield of about 35%.

Lysozyme water content

The water content of lyophilized lysozyme was determined using the following procedure. Three small weighing bottles with stoppers were placed in a vacuum oven at 110°C for 18 hours. The bottles were removed, placed in a desiccator and weighed every half hour for two hours. The bottles adsorbed a small amount of water. By extrapolation to zero time, this method allowed the estimation of empty bottle masses.

A solution of 0.5 g/5 ml of lysozyme in deionized water was prepared. Of this, one ml, or 0.1 gram, was pipetted into each weighing bottle. The bottles and protein samples were lyophilized and then placed in the oven at 110°C for 18 hours under vacuum, and in the same way as in the previous step, were removed, placed in a desiccator and weighed every one-half hour for two hours. The weighing bottles and dried protein were cycled through the vacuum oven and desiccator until a constant weight was achieved.

Gel electrophoresis (SDS-PAGE)

Purity of the three soluble fractions retained following cation-exchange chromatography was verified by gel electrophoresis. Polyacrylamide gel was used as the molecular-sieve supporting medium. Proteins were treated with an

ionic detergent, Na dodecylsulfate (SDS), which bound the proteins in a constant weight ratio. Intrinsic charges on the protein were insignificant compared to negative charges on the bound detergent. Under the influence of an applied electric field, the SDS-protein complexes moved through the gel as a function of charge density. The separation which resulted was essentially based on protein molecular weight.

A 10% polyacrylamide gel, along with an appropriate series of molecular weight markers, was used. Standard procedures were followed (Appendix A)[65].

Polymer sample preparation

High surface area samples:

High-surface area samples of polystyrene [Aldrich, MW 280,000 (GPC)], poly(co-styrene-butyl methacrylate) [Scientific Polymer Products, butyl methacrylate content - 50%, MW 200,000(GPC)], and poly(co-styrene-allyl alcohol) [Scientific Polymer Products, alcohol content 5.4-6.0%, MW 3000 (GPC)] were prepared. Samples were prepared by adsorbing polymer from solution onto finely divided fumed silica (Degussa, 130 m^2/g), separating the polymer-adsorbed-silica from the polymer solution, and drying.

Preparation of silica: To remove surface water and to standardize the surface with respect to the type of functional group present, the silica was heated at 900°C for 10 minutes under vacuum. The heat-treated silica was kept sealed in a desiccator until used.

High-surface area polystyrene: A two-percent solution of polystyrene in cyclohexane was brought to 65°C. Silica in the ratio of 100 mg/100 ml was added to the solution and the mixture was vigorously stirred for twenty minutes. The mixture was passed through a coarse $(10-15\mu m)$ fritted glass filter to separate the sample from the solution. The sample was placed in an

oven at 110°C under vacuum for 24 hours, removed and ground with a mortar and pestle, and returned to the oven at 110°C for 24 hours under vacuum. The dried polymer sample was stored in a capped glass bottle.

High-surface area poly(co-styrene-butyl methacrylate) and high-surface area poly(co-styrene-allyl alcohol): A one-percent solution of copolymer in toluene was prepared and brought to 100°C. Silica was added in the ratio 100 mg/100 ml, the solution was stirred for twenty minutes, and the sample was separated, dried and stored as for polystyrene, above.

Flat samples:

Flat polymer samples for contact angle measurements and Wilhelmy plate studies were made beginning with undoped silicon wafers of crystallographic orientation [100] which had been highly polished on both sides (Virginia Semiconductor). A silicon-oxygen layer of about 400 Angstroms was grown on the wafers by heating in dry oxygen at 1000°C for one hour. Due to the particular crystallographic orientation, the wafers were then easily broken along etched lines into the various rectangular pieces needed.

Static and dynamic contact angles, to be reproducible, required careful handling of sample surfaces. The oxide-covered wafers were cleaned by first heating in a solution of five parts deionized water, one part ammonium hydroxide and one part 30% hydrogen peroxide at 80°C for 20 minutes, and then rinsing in deionized water. This procedure ensured the removal of organic material from the oxide surface. The wafers were then placed in a solution of five parts deionized water, one part hydrochloric acid and one part 30% hydrogen peroxide at 80°C for 20 minutes and rinsed. This second step removed heavy metal atoms from the surface. At this point, if the wafers were not adequately rinsed in deionized water, no reproducibility in contact angle measurements was possible. This was likely due to the continued presence of

ions from the cleaning procedure. To remove as many surface ions as possible, the resistivity of the rinse water was monitored until it matched that of uncontaminated deionized water. The wafers were then dried at 110°C for 18 hours under vacuum.

Polystyrene layers were added to the oxide-covered wafers by adsorption from cyclohexane at 65°C for 20 minutes. The wafers were rinsed in cyclohexane and dried at 110°C for 18 hours under vacuum.

Styrene/butyl methacrylate and styrene/allyl alcohol layers were added by adsorption from toluene at 100°C for 20 minutes. The wafers were rinsed in toluene and dried at 110°C for 18 hours under vacuum.

Verification of adsorption of polystyrene by silica

Verification of adsorption was determined by noting a shift to lower wavenumbers of the surface silanol group after sample preparation.

A series of polystyrene/carbon tetrachloride solutions was prepared, ranging in concentration from 0.001% to 3.0%, and heated to 65°C. Heat-treated silica was introduced to each in the ratio 100 mg/100 ml and the mixtures stirred for 20 minutes. Samples were separated from solutions by passing the mixtures through a fritted coarse glass filter. Samples were dried overnight at 110°C in vacuum, and then ground with a mortar and pestle.

Spectra of each ground sample were made using a Perkin Elmer Model 1740 Fourier Transform Infrared Spectrometer.

Determination of surface area

Surface areas of high surface area substrates were determined using a

Quantasorb sorption analyzer. A nitrogen/helium (0.293:1) mixture at liquid nitrogen temperature was used as the adsorbate. Pretreatment included a one hour outgassing with nitrogen at 150°C.

Adsorption isotherm

Ratios of peak heights from infrared spectra were used to determine the amount of adsorbed polymer or copolymer per gram of silica. The heights of the polymer peak at 700 cm^{-1}, attributed to out-of-plane deformation of the styrene aromatic group[66], and the silica peak at 1100 cm^{-1}, attributed to stretching of bulk Si-O-Si groups[67] were measured in absorbance relative to background at 1450 cm^{-1}.

Calibration curves were made by taking spectra of mixtures of ground polymer or copolymer and silica in various proportions.

Determination of minimum polystyrene thickness required to mask silicon oxide properties

Because of the composite nature of the high-surface area samples made for use in the microcalorimeter, it was necessary to ensure that any properties influencing lysozyme adsorption were due solely to the polymer part of the sample without contribution from the silica. This was accomplished by determining the minimum polymer layer thickness at which contact angles became constant. Flat polystyrene samples, made using oxide covered silicon wafers as previously described, were used for this purpose.

Thicknesses of the silicon oxide layer of a series of 1cm x 1cm cleaned wafer pieces with no polymer layer were measured using a Gaertner ellipsometer and a one-layer software program for the silicon/silicon oxide system. This

instrument and software allows the measurement of extremely thin silicon oxide layers of assumed refractive index 1.464 to an accuracy of ±3 Angstroms.

Very thin polystyrene layers were placed on the oxide surfaces by adsorption from extremely dilute solutions in cyclohexane. A second series of ellipsometer measurements was made. Subtracting the thickness of the oxide layer allowed an estimation of the thickness of the polymer.

Half of the wafers were placed horizontally in a small glass container with flat sides and optically smooth glass, and immersed in distilled octane. A small (0.1μl) drop of distilled, deionized water was placed at the center of each wafer with a microliter syringe. Contact angles were measured using a Gaertner goniometer.

The remaining wafers were placed in a second glass container and immersed in distilled, deionized water. Small octane drops were placed on the underside of each wafer and the contact angles measured. Each series of contact angles was plotted against polystyrene layer thickness.

Time of immersion of wafer in solvent or time of contact of drop with surface was not a variable in this study. Immersion times were generally a few minutes and contact angles were measured generally within 15 seconds of placement.

TEM study of silica and of high-surface area polystyrene

Transmission electron micrographs of plain silica and of polystyrene-covered silica were taken to gain information about the thickness of the polystyrene layer.

To enhance electron density contrast of the carbon-containing polystyrene relative to the carbon film support grid, a staining agent was used. Ruthenium tetroxide is an oxidizing agent which apparently binds the phenyl group of

polystyrene[68]. A carbon grid dusted with a small amount of polystyrene-covered silica was vapor stained for one hour using a solution of 0.5% RuO_4 in deionized water.

A similar grid for plain silica was prepared, but was not vapor stained as silica required no contrast enhancement.

Electron micrographs were taken with a JEOL 4000 electron microscope at an accelerating voltage of 400 kV.

Wilhelmy plate

Wilhelmy plate studies were carried out to verify that polymer surfaces have different properties in different environments.

This study required the measurement of very small forces exerted on flat plates by water during vertical plate movement. These measurements were accomplished by fitting an Instron Universal Testing machine with a 10 gram load cell and by use of an auxiliary plotter connected to the circuitry of the Instron's chart recorder. This setup allowed a reversible, variable speed vertical drive for plate movement, and a one-way sweeping variable speed recorder with a sufficiently small full scale range of about 3 grams. The system was calibrated using paper clips of known masses.

A one inch by one inch cleaned oxide covered silicon wafer was coated with polystyrene by allowing adsorption from a 2% solution in cyclohexane, followed by drying at 110°C for 18 hours under vacuum. This treatment resulted in a fairly thick layer on the order of micrometers. The wafer was attached by wire to the load cell and lowered at a rate of 0.5 cm/minute into a beaker of distilled, deionized water to a distance of about 0.8 cm. The direction of the Instron was then reversed, and the plate pulled upward from the water at the same rate. This procedure resulted in a recorded hysteresis loop. The

plate was then immersed in distilled, deionized water and removed at varying intervals to be tested on the Instron. Water used for soaking was changed after each test. Testing continued up to 30 hours of immersion time.

Additional plates were covered with layers of poly(co-styrene-methacrylate) and poly(co-styrene-allyl alcohol) by allowing adsorption from 1% solutions in toluene. This procedure again resulted in fairly thick layers. The above testing procedures were repeated.

A typical hysteresis loop is shown in Fig. 1. The initial increase in force recorded as the plate touched the water was a result of the mass of water present in the meniscus due to wetting. As the plate was immersed further, the force decreased from buoyancy effects. The change in slope represents the point where the advancing contact angle reached a maximum, after which it remained constant. As the plate was removed from the water, the force increased from decreasing buoyancy effects. The change in slope represents the point where the contact angle, which were the receding contact angles, reached a minimum.

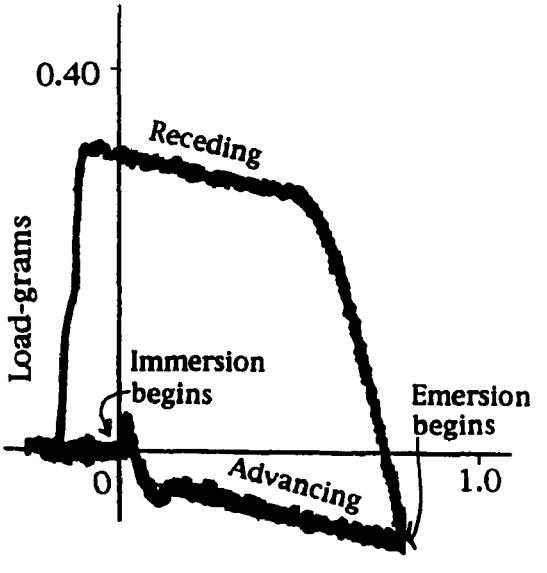

Fig. 1. Wilhelmy hysteresis loop.

Advancing and receding contact angles were calculated from the forces obtained at the point of zero depth of immersion of the plate in the water. At this point, buoyancy effects could be ignored and the equation

$$F = mg + P\gamma_L \cos\theta \tag{7}$$

was applicable[69].

Vibrations were present during each test as a result of the operation of the Instron. To minimize vibrations in the liquid, the beaker of water was set on a one-quarter inch thick stack of rubber sheeting.

Pendant drop procedure

The experimental apparatus used for measuring surface tensions of molten polymer drops is shown in Fig. 2. The setup consisted of two vertical 10 inch long aluminum tubes situated one inside the other. A glass syringe was placed so that a polymer drop could be formed midway along the length of the inner tube. Holes were drilled through both tubes at this point for viewing, and quartz plates were secured over the viewing holes of the inside tube. Temperature was controlled by an Omega Series 920 Solid State Controller attached to band heaters situated above and below the viewing holes. This arrangement allowed temperature at the drop position to be maintained to within $\pm 0.2^{o}C$ of the set point up to $170^{o}C$. Temperature at the drop position was monitored with a thermocouple placed adjacent to the drop. Finally, to maintain a relatively oxygen-free environment within the inside tube, a dry nitrogen port was positioned at the upper end of the apparatus to allow for continuous flushing.

To form drops, the polymer-filled syringe was first positioned in the apparatus and allowed to sit at a temperature suitable for the polymer to become molten. At this point, enough material to form a drop with a neck was

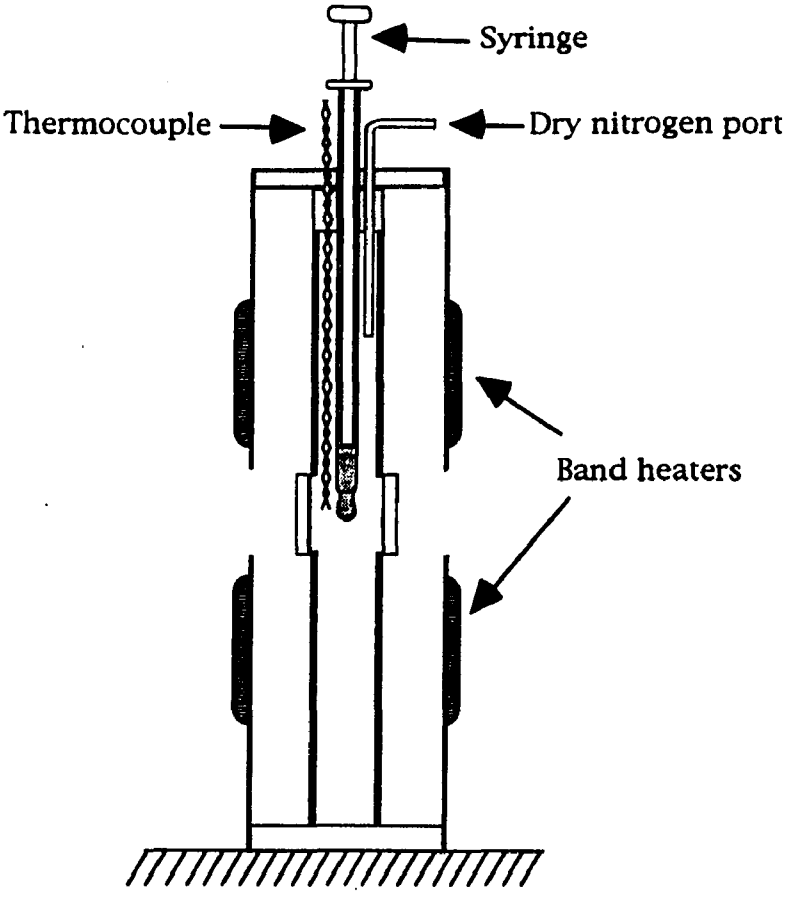

Fig. 2. Cross-sectional sketch of pendant drop apparatus.

extruded by depressing the plunger. The drop was allowed to stand until it gained a symmetrical profile and the surface appeared smooth. The temperature was then dropped to the starting temperature of interest.

Shape factors for the drop were measured at a series of increasing temperatures. At each temperature, the drop was allowed to sit until the shape factor did not change. It was assumed that at this point the drop was at equilibrium. To monitor the change in shape factor, photographs were taken at various time intervals using a Pentax 35mm camera with a close-up lens and back lighting.

The temperature range over which each material was tested was chosen to provide reasonable times for drop equilibration. Polystyrene (MW 280,000) was quite viscous and was tested at higher temperatures than was poly(co-styrene-allyl alcohol) (MW 3000), which was fluid just a few degrees above T_g. At the starting temperature for each material, the drop was allowed to stand for 18 hours. It was assumed that this was sufficient time for equilibration at the relatively low starting temperature. As the results showed good linearity, this assumption was likely adequate. At relatively high temperatures where the material was fluid, and at all temperatures for poly(co-styrene-allyl-alcohol), five minute equilibration times were assumed to be sufficient.

Shape factors were determined from measurements of photograph negatives projected over a large distance. This condition was sufficient to follow the changes in drop profile.

Surface tensions were calculated from the equation:

$$\gamma = \frac{g\rho(d_e)^2}{H} \quad , \tag{8}$$

where g is the gravitational acceleration, ρ the density of the drop, d_e the equatorial diameter of the drop and 1/H a correction factor determined by the shape of the drop[70]. Andreas[71] tabulated 1/H as a function of the shape parameter S defined as the ratio d_s/d_e, where d_s is the horizontal diameter of the drop measured at a distance d_e up from the bottom of the drop.

Determination of polymer densities as a function of temperature

The density of a nonporous solid can be found by using a pycnometer of known volume and a non-interacting liquid of known density. The liquid chosen for this study was polydimethylsiloxane (1000 centistokes, Petrarch), which is stable in the temperature range of 70-170°C. It also did not appear to

interact with the polymers studied over the length of time required to complete measurements.

Volume of pycnometer as a function of temperature:

An empty 10 ml pycnometer was placed in an oven at 70°C for one hour, removed, placed in a desiccator for 20 minutes and then weighed. The pycnometer was filled with polydimethylsiloxane and returned to the oven with the cap off. After two hours, the cap was replaced, the overflow wiped away, and the pycnometer was returned to the desiccator. After 20 minutes it was again weighed. This procedure, along with density vs temperature data supplied by Petrarch for polydimethylsiloxane, allowed the determination of the pycnometer volume and was repeated at temperature intervals up to 170°C. Temperature was followed by monitoring voltage using a Keithley 179 digital multimeter and a copper-constantan thermocouple, one end of which was placed inside the pycnometer, and the other in an ice water reference.

Polymer densities as a function of temperature:

Five grams of polymer or copolymer were placed in the pycnometer along with enough polydimethylsiloxane to produce overflow upon heating. Heating and weighing procedures were similar to that described above. Polymer densities were determined from the following relation:

$$(\text{density})_{\text{total}} = (\text{vol. fx.})_{\text{liq.}} \cdot (\text{density})_{\text{liq.}} + (\text{vol. fx.})_{\text{polymer}} \cdot (\text{density})_{\text{polymer}} \quad (9)$$

Microcalorimetry

Heats of adsorption were obtained in a Tian-Calvet conduction microcalorimeter at 37.0°C, Fig. 3. This instrument was capable of reliably measuring heat outputs of 0.1 mcal hr^{-1} or less. It consists of twin reaction cell chambers positioned symmetrically about the vertical axis of a large aluminum block. Resistance coils are wrapped around the block, and its temperature is regulated by an Athena model 51 solid state proportional temperature controller. Along the sides and bottom of each cell chamber is located a thermoelectric pile which serves to transfer heat from the reaction

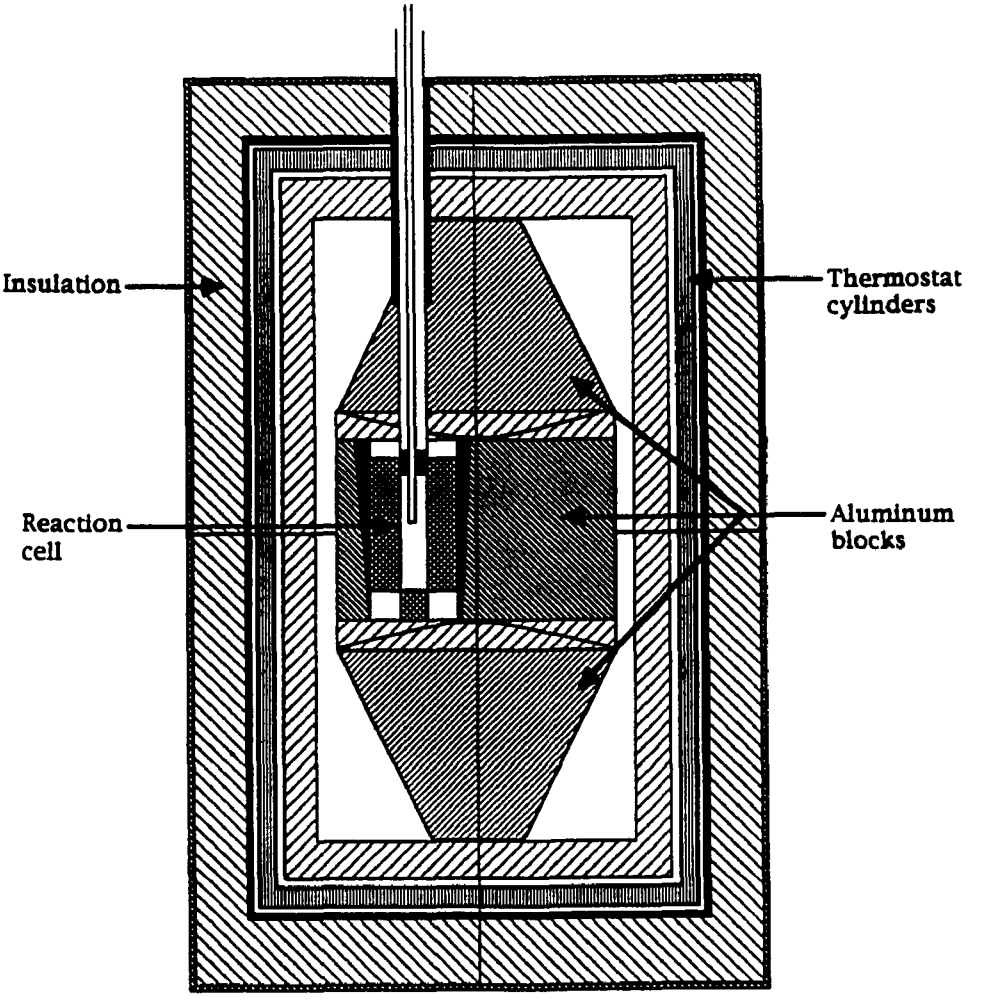

Fig. 3. Cross-sectional sketch of Tian-Calvet microcalorimeter.

chamber to the surrounding aluminum heat sink. The pile consists of identical thermoelectric junctions, each separated from the other by equal distances. The couples are attached perpendicularly between the cell chamber wall (internal boundary) and the heat sink (external boundary), and a sufficient number is used so that each junction covers only a very small part of the wall area.

Let each junction occupy an area S, and the area between junctions be S'. Let θ_i be the temperature of a given junction at the internal boundary. Since S + S' is small, θ_i may be considered to be the temperature of the junction i and surrounding area, regardless of temperature variations at other points on the internal boundary[72].

The heat flux from S + S' consists of that conducted by the thermocouple wire,

$$\phi_i = c(\theta_i - \theta_e) \ , \tag{10}$$

where c is the thermal conductivity of the wire and θ_e is the temperature of the heat sink, plus heat radiated and convected from the surface,

$$\phi_i' = \gamma(\theta_i - \theta_e) \ , \tag{11}$$

where γ is the emissivity of the surface, for a total flux of

$$\phi_i + \phi_i' = (c + \gamma)(\theta_i - \theta_e) \ . \tag{12}$$

For n thermocouples, the total heat flux is

$$\Phi = (c + \gamma) \sum_{i=1}^{n} (\theta_i - \theta_e). \tag{13}$$

The emf generated in a thermocouple is

$$e_i = \varepsilon_o(\theta_i - \theta_e) \ , \tag{14}$$

where ε_o is the thermoelectric power of the thermocouple. Since all of the

couples are connected in series, the total emf is

$$E = \varepsilon_o \sum_{i=1}^{n} (\theta_i - \theta_e). \tag{15}$$

The combination of equations 13 and 15 gives

$$E = \frac{\varepsilon_o}{(c+\gamma)} \cdot \Phi \tag{16}$$

Therefore, the emf generated by the thermoelectric pile is proportional to the total heat flux from the internal boundary. This equation is valid on the condition that the temperature at the external boundary, θ_e, remains constant.

Above and below the reaction cell chambers and aluminum block are positioned two large truncated aluminum cones. This three-block assembly is symmetrically located in a thick insulated jacket consisting of several concentric metal canisters. The purpose of this arrangement is to transform lateral thermal perturbations into vertical perturbations equally shared by the twin elements. For example, a perturbation produced by a change in room temperature, if not entirely diffused by the insulated jacket, would be conducted away from the cone tops and become a parallel flux through the center block. The above assembly thus results in the temperature at the external boundaries of the two cell chambers being identical at any given moment. Then, by connecting the thermoelectric piles of the two elements in opposition, no net electrical output, or a baseline of long-term stability, results.

A Keithley Model 148 nanovoltmeter-amplifier and a Brown Electronik Honeywell multipoint potentiometric recorder were used to record the microcalorimeter output. The nanovoltmeter-amplifier had a noise level of less than 10^{-9}V and a zero drift of less than 10^{-8}V over a 24-hour period. It is also largely unaffected by ordinary temperature and humidity changes, and

by vibrations. The most sensitive scale of the instrument is 20nV full range, although for this work the $3\mu V$ full range scale was used. The Brown recorder was chosen for its good zero stability.

The resulting sensitivity of the above assembly is limited mainly by Johnson noise, which is a function of resistance of the thermocouple wiring and amounts to about 10 to 15nV.

Recorded curve areas were measured using a Keuffel and Esser Model 620000 compensating polar planimeter. This instrument measures areas to $0.01in^2$ and is capable of reproducing areas to within 1%.

Calibration:

Each cell chamber was calibrated by passing a known amount of current through copper-constantan coils of known resistances for a measured period of time. Currents were measured using a Keithley 179 digital multimeter. Each run resulted in an initial increase in the voltage output of the recorder which subsequently decayed to zero. When the recorder trace reached baseline, the area under the curve was measured with a planimeter. This area was assumed to correspond directly with the heat produced by the coil. This quantity was calculated as follows:

$$Q = R\, i^2 t\,, \tag{17}$$

where Q was the heat generated in calories, i the measured current, and t the time in seconds. Curves with areas of different magnitudes were generated by varying the time of current application. Linear heat vs area curves for the 3μV scale and a chart speed of 6"/hour resulted.

Reaction cell assembly:

A two-tube setup was used to allow mixing of protein and polymer within the calorimeter, Fig. 4. The assembly consisted of highly polished stainless steel cylinders (1.64 cm o.d. and 8.22 cm in height). The upper ends of the

cylinders were threaded to accommodate a threaded Teflon plug. A 61 cm long glass tube of 5 mm diameter was attached to the Teflon plug for the purpose of raising the assembly and lowering it into the calorimeter.

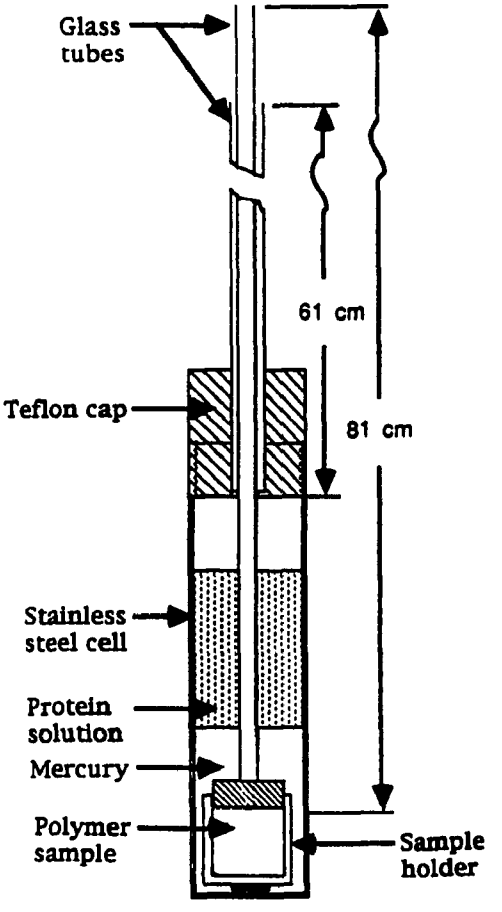

Fig. 4. Two-tube reaction cell assembly.

The polymer sample, prewetted for 48 hours in deionized water to achieve sample equilibration and to eliminate a large wetting heat, was placed in a small glass cup along with 2 ml of deionized water, almost completely filling the sample holder. Sufficient sample was added to provide a surface area of 4.65 m^2. The polymer sample, being less dense than water, remained at the upper end of the sample holder. A Teflon cap, attached to an 81 cm long glass tube of 3 mm diameter, loosely sealed the sample cup. The sample cup, cap and tube were placed at the bottom of the stainless steel cylinder and weighted

down while enough mercury to cover the sample holder was added. The mercury served to keep the sample and protein solution separate until the time of mixing, and with its high surface tension, did not penetrate capillary spaces between the Teflon cap and sample holder. Above the mercury, 4 ml of protein solution was added. The cylinder was sealed by threading on the Teflon plug, and the above procedure was repeated for the second cell assembly.

The cell assembly operated in the following way. After being lowered into the calorimeter, the calorimeter and contents were allowed to equilibrate for four hours. Upon reaching a stable baseline on the chart recorder, reaction in one cell was initiated by slowly raising the inner tube with a synchronous motor. This allowed the sample holder to rise due to the buoyancy of the mercury. At the point where the sample holder sat on the mercury surface, its cap was lifted and allowed to rise 5 mm more. The polymer sample, being less dense than water, floated upward through the protein solution. The resulting recorded curve was then converted to an enthalpy value using calibration results. During this procedure, the second cell assembly acted as a tare or reference for the assembly containing the reaction. After the recorder trace again reached baseline, the first cell assembly was used as the reference for a reaction allowed to occur in the second assembly.

Some precautions were necessary in the above procedures. In order to lessen the time required for the calorimeter to reach equilibrium, the two cell assemblies were lowered into the calorimeter together. To minimize baseline drift during a run, the cell setups were made to be as identical as possible, i.e. the same amount of mercury and solvent, and protein solutions very close in concentration. This was not difficult on the $3\mu V$ scale, as no discernible baseline drift was noted over a 24 hour period, though room temperature fluctuated between 16°C and 20°C. To minimize heats generated by bubble

movement, the sample cups were filled as completely as possible. To prevent the sample holder from failing to rise, a thin Teflon spacer was placed beneath it. Finally, cleanliness and dryness of all assembly components, and their careful manipulation during runs was critical in eliminating exothermic artifacts.

Preparation of lysozyme solutions

Protein solutions for microcalorimetry were prepared in phosphate buffer with purified, lyophilized lysozyme. Solution concentrations were determined from an optical density reading at 280nm on a Beckman ACTA III Spectrometer along with a calibration constant. A calibration curve was prepared from optical density readings of a series of dilute lysozyme solutions. Solutions were stored for up to two days at 4°C in capped glass bottles sealed with Para-Film.

Amount of lysozyme adsorbed by high-surface area polymer substrate

The amount of lysozyme adsorbed by polymer substrate during reaction in the calorimeter was calculated using absorbance measurements of the supernatant protein solution at 280nm. Since lysozyme absorbs very strongly at 280nm, this method had sufficient sensitivity to detect very small concentration differences.

The Beckman instrument was reliably able to detect a lysozyme concentration difference of less than 0.001%. Above the lowest concentrations, it was necessary to make dilutions, which were done using Eppendorf adjustable digital pipettors.

After reaction in the calorimeter, cell contents were centrifuged to separate solid from liquid. Solid settled at both ends of the centrifuge tube. As the

density of lysozyme just exceeds 1.0 g/cm^3, it is likely that the polymer substrate existed in a range of densities. This result also suggested that a fraction of lysozyme/polymer complex had a density very near that of the protein solution, and did not move during centrifuging. It was necessary to remove this fraction, which absorbed strongly at 280nm. The fraction was removed using Millex- GV_4 Durapore filters (Millipore), pore size $0.22\mu m$, before measurement of absorbance. If a dilution was necessary, filtering was done after the dilution was made.

The Millex filter, while only 4 mm in diameter, had a very high surface area, and adsorbed unbound lysozyme during filtering. Three filters were calibrated for amount adsorbed by measuring the difference in optical density before and after filtering dilute lysozyme solutions. To within two figures of agreement, a filter retained 5.2% of unbound lysozyme during filtering.

The concentration of lysozyme in a filtered solution was determined from the following relation:

$$\text{Conc.}(\%) = \frac{(\text{optical density})\cdot(\text{dilution factor})\cdot(\text{volume of solution})}{(\text{filter calibration constant})\cdot(\text{spectrometer cal. constant})\cdot 100} \qquad (18)$$

FTIR - conformational changes

Infrared spectra of high surface area polymer samples with adsorbed lysozyme were studied for evidence of protein conformational changes. Mulls in mineral oil were prepared from samples obtained from calorimeter runs. Substrate/lysozyme complex was separated by centrifuging, rinsed once with deionized water and lyophilized. Lyophilization eliminated interference from water peaks.

A Perkin Elmer model 1740 Fourier Transform Infrared Spectrometer was used. Peak height ratios in absorbance of the amide bands at 1660cm^{-1} and 1540cm^{-1} were compared to those of unadsorbed lyophilized lysozyme. To more clearly see the amide bands of the adsorbed protein, nearby and overlapping peaks were subtracted. For example, from a spectrum of the silica/ polystyrene/lysozyme/mineral oil system was subtracted a spectrum of silica and polystyrene in mineral oil.

CHAPTER IV

RESULTS AND DISCUSSION

Protein preparation

Lysozyme as obtained from Sigma was not homogeneous. Purification revealed five fractions by chromatography on a column of Bio-Rex 70, in addition to a large insoluble fraction, Fig. 5. These results are very similar to those obtained by Saxena[64] and by Stevens[73] who purified hen egg white lysozyme (Worthington Biochemical) under similar conditions.

Several possible explanations have been proposed for the multiple forms. Jolles has suggested that deamidation of asparagine and glutamine residues may occur during the alkaline conditions used in crystallization of the protein[74]. This alteration would lower the net positive charge at neutral pH, and therefore, the affinity of the enzyme for the cation exchange resin. Fractions 1, 2, 3, 4 and 5 may differ in the number of amide groups per molecule.

A second possibility is that the same alkaline conditions resulted in the rearrangement of disulfide bonds in native lysozyme. Anfinsen showed that active lysozyme results from only one arrangement of four disulfide bonds from the eight half-cystine residues present in the lysozyme molecule[75].

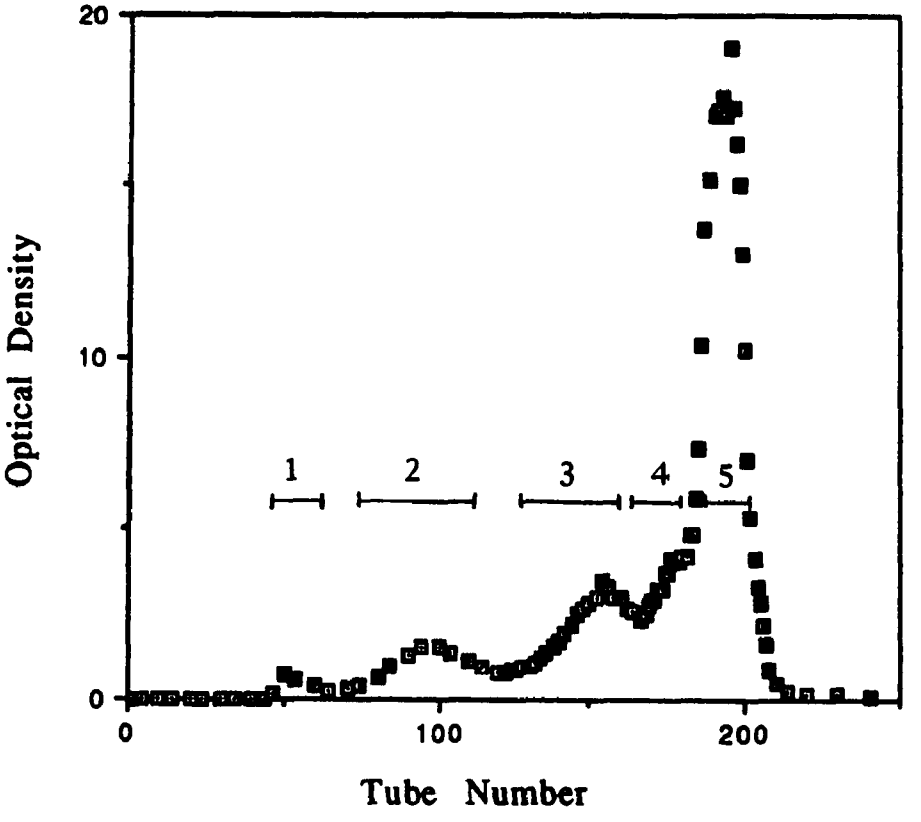

Fig. 5. Fractions obtained by chromatography of lysozyme on Bio-Rex 70 at 25°C and pH of 7.14.

Multiple forms have also been found in duck egg white lysozyme. Analysis by starch-gel electrophoresis suggested that the multiple forms were due to more than one allele at a single locus[76]. Jolles observed, during structure studies of hen egg lysozyme, that residue 118, threonine, was actually present as serine in about 5% of cases[77].

Fractions 3, 4 and 5 were found to be indistinguishable in molecular weight from the lysozyme standard in SDS-PAGE gel electrophoresis, Fig. 6. Stevens obtained similar results using osmotic pressure measurements[73]. Stevens also reported that from enzyme activity measurements using *Micrococcus lysodeikticus* cells, fraction 3 was nearly as active as fraction 4 (0.937 vs 1.010), whereas fraction 5 possessed less specific activity (0.772 vs 1.010).

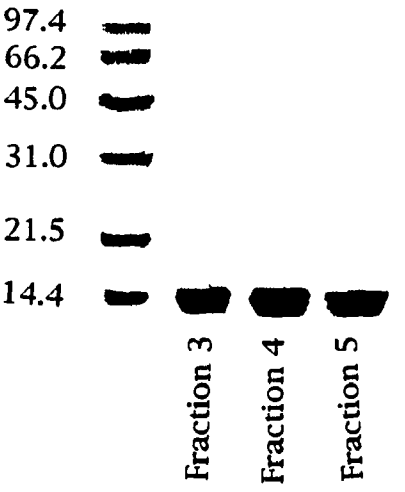

Fig. 6. SDS-PAGE gel electrophoresis of lysozyme fractions 3, 4 and 5.

Fractions 3, 4 and 5 were combined for this work. Large amounts of protein were required, and no method of improving peak resolution was found in the literature.

Water content of the lyophilized lysozyme was determined to be 8.90%, Fig. 7.

Sample preparation

The infrared spectrum of nonporous fumed silica in the as-received state showed a broad absorption band centered around 3400cm^{-1} attributable to adsorbed water vapor, and a lower intensity, asymmetrical peak at 3750cm^{-1} attributable to the fundamental stretching frequency of a hydroxyl group attached to a silicon atom on the surface of the silica[78], Fig. 8a. The width and asymmetry of this peak indicate a distribution of configurations of the silanol group.

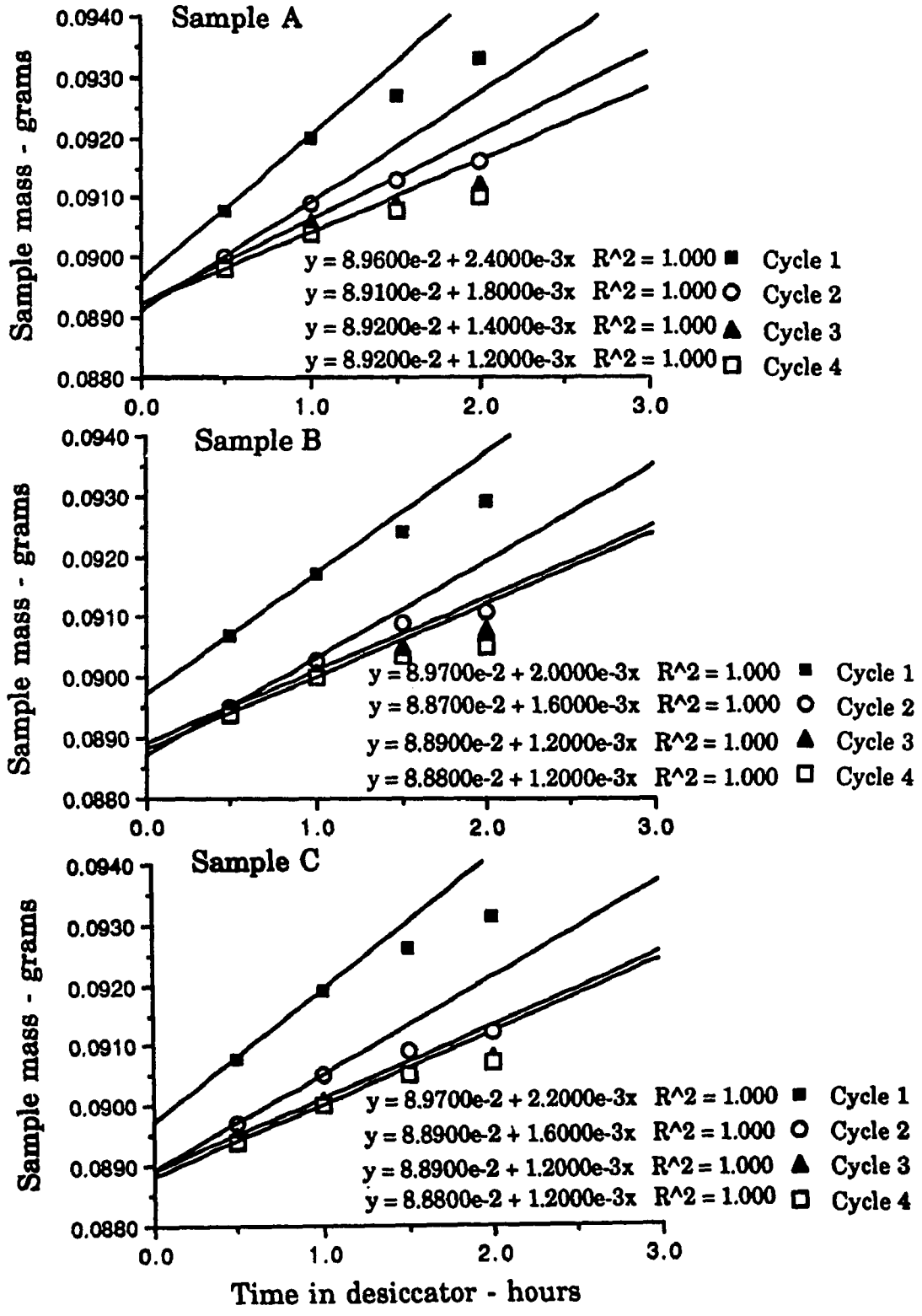

Fig. 7. Determination of water content of lyophilized lysozyme.

Heat treatment under vacuum resulted in large part in the disappearance of the water peak and an increase in symmetry of the silanol peak at 3750cm^{-1}, Fig. 8b. These changes indicate that adsorbed water associates directly with silanol groups, and that its removal leaves the silanol groups with essentially identical environments.

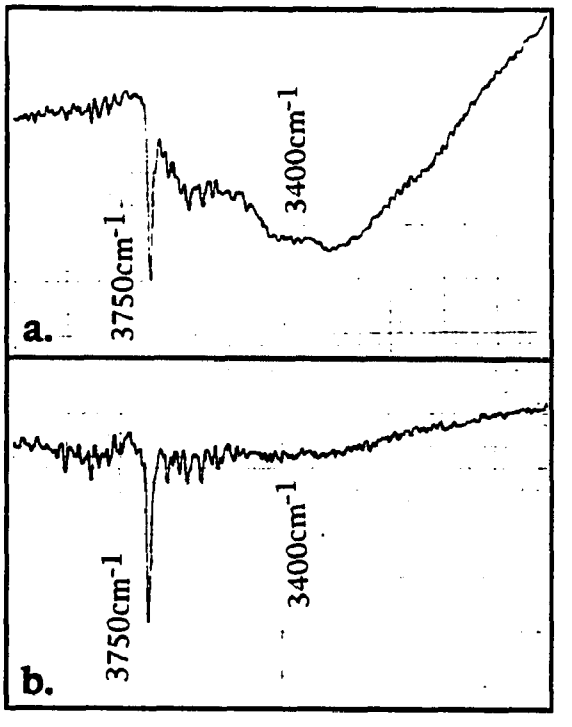

Fig. 8. Infrared spectra:
a. Silica, as-received, and
b. Silica, heat-treated at 900°C for 10 minutes in vacuum.

Adsorption of polystyrene by silica was verified by noting a shift to lower wavenumbers of the surface silanol group after sample preparation. The shift indicated an increase in the effective mass involved in the particular group vibration of interest, and is qualitative evidence of physical bond formation.

The series of spectra in Fig. 9. show the progress of adsorption. Little adsorption occurred from very dilute polystyrene solutions such as 0.001%. The appearance of the small peak at 3588cm^{-1} indicates that a few surface

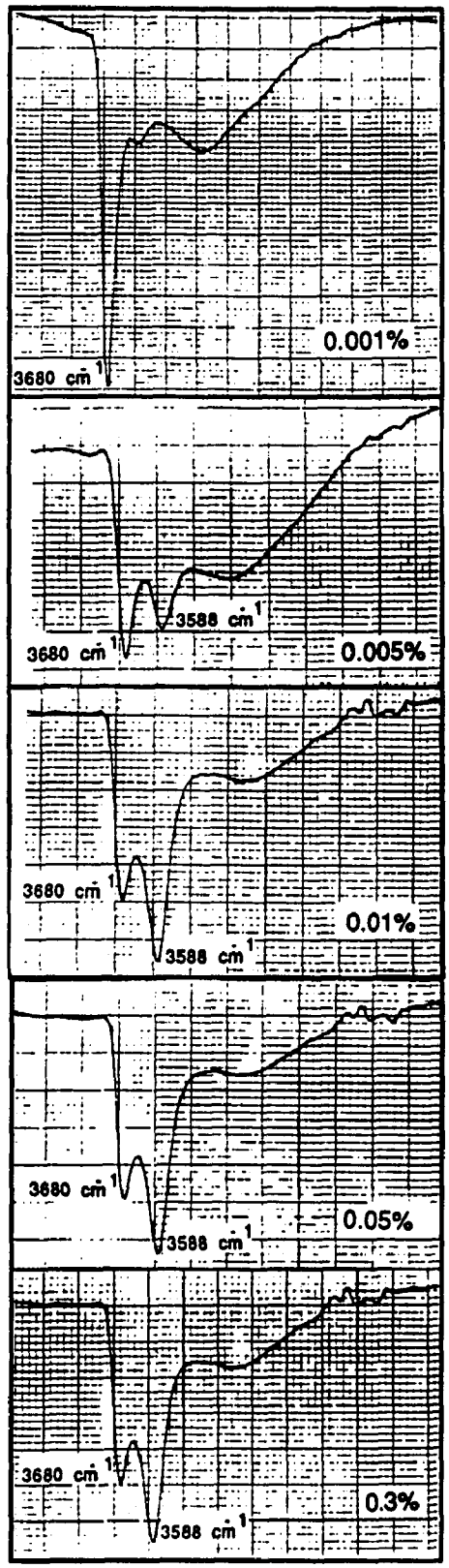

Fig. 9. Infrared spectra showing progress of adsorption of polystyrene by silica at concentrations of 0.001-0.3% in carbon tetrachloride. The shift of the silanol peak indicates physical bond formation with polystyrene.

silanol groups were physically associated with polystyrene. Relative peak heights changed as solution concentration increased, indicating a larger fraction of bonded surface groups. No apparent change in ratio was noted at concentrations above 0.01%. This probably indicates that some silanol groups remained unbonded due to steric reasons. It also means that, given the uniformity of the silanol groups in the starting condition, uniform coverage of the silica surface by polystyrene was achieved.

The polystyrene adsorption isotherm was of the high-affinity type, with a limiting plateau of 0.70 g/g silica starting at a low bulk concentration of 0.02%, Fig. 10.

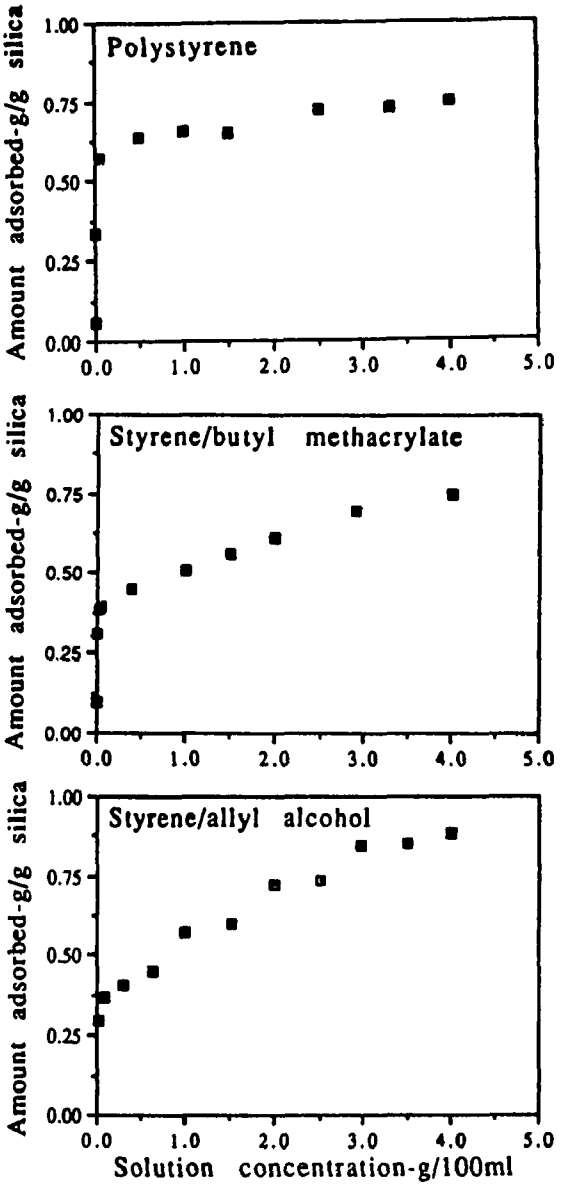

Fig. 10. Adsorption isotherms of sample polymers on silica.

Isotherms of copolymers did not show limiting plateaus. Cohen-Stuart has attributed isotherms with continuously increasing adsorbed amounts to broad molecular weight distributions[79]. Polydispersity indexes for poly(co-styrene-butyl methacrylate) and poly(co-styrene-allyl alcohol) are 1.88 and 2.33 respectively[80]. The index for polystyrene was not available.

Surface areas of polystyrene, poly(co-styrene-butyl methacrylate) and poly(co-styrene-allyl alcohol) samples for microcalorimetry were determined to be 71, 93 and 85 m^2/g, respectively.

The electron micrograph of uncoated silica shows spherical particles of about 15 nm diameter fused into aggregates, Fig. 11. Aggregates ranged in size up to several hundred nanometers.

Polystyrene-coated silica appeared as clumps of approximate diameter 50 nm fused into clusters. The smallest cluster found on the grid measured 350 nm.

Polystyrene layer thickness could not be determined from the micrograph. Calculation from adsorption isotherm data predicts a thickness of 50 nm, assuming a density of 1.08 g/cm^3, and even coverage of silica.

As noted in Figure 12, contact angles remained constant beyond a minimum polymer layer thickness. At the polymer/octane interface, dispersion interactions were predominant due to the highly nonpolar nature of octane. The change in contact angle of a water droplet with increasing polystyrene layer thickness reflected changing contribution to dispersion interactions by the silicon oxide. Similarly, the change in octane contact angle at the polymer/water interface reflected the changing contribution of silicon oxide to polar, as well as dispersion interactions.

Surface mobility probably changed with polymer layer thickness. Polymers form loops and tails upon adsorption. An increase in surface

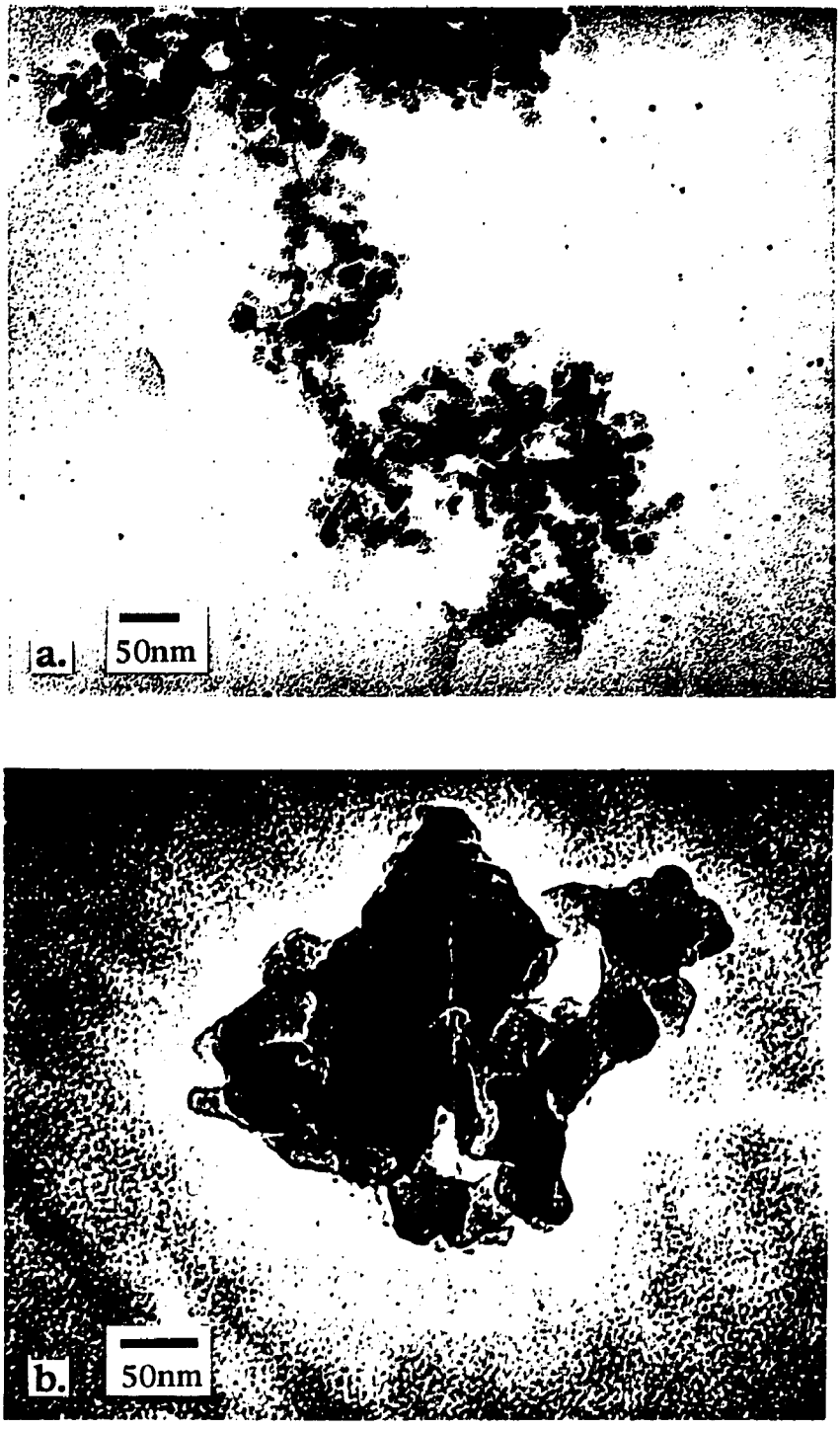

Fig. 11. Transmission electron micrographs:
a. Uncoated silica, 120,000X
b. Polystyrene-coated silica, 150,000X

configurational entropy will influence surface and interfacial free energies, and therefore contact angles.

It appears that a polystyrene layer thickness of 40 Angstroms was sufficient to provide a surface uninfluenced by silicon oxide properties or by polymer layer thickness.

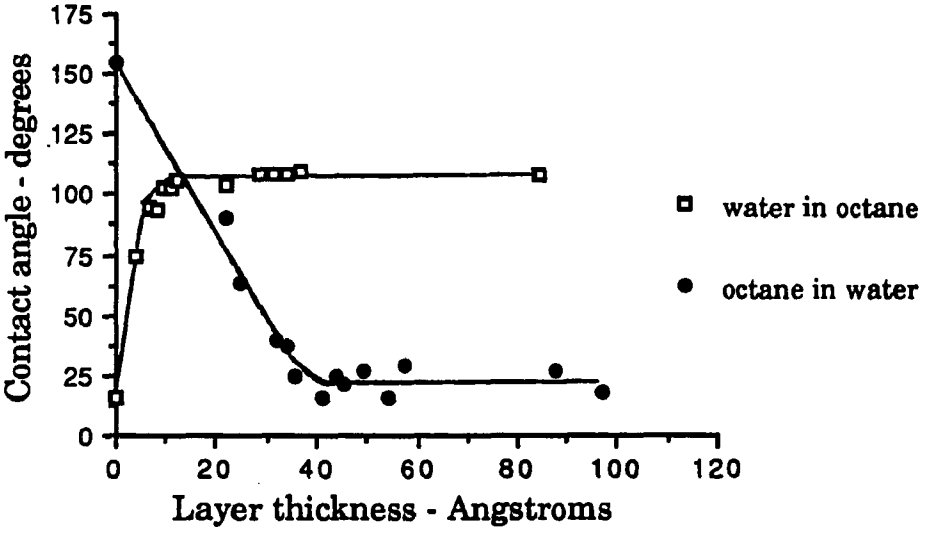

Fig. 12. Contact angles vs thickness of polystyrene layer.

Kessaissia et al.[81] determined from contact angle measurements of water on silica surfaces grafted with alkyl chains of varying length that the polar nature of silica was masked as the chain length approached 20 carbons. This represented a thickness of about 30 Angstroms if the chain extended perpendicularly from the surface.

Interfacial energies

A surface is a discontinuity and is defined wherever a phase terminates. The phase may terminate at a vacuum or at the surface of another phase. The surface formed where two phases meet is an interface.

The major thermodynamic quantity which characterizes a surface or an interface is the reversible work, γ, needed to create unit area of surface at constant temperature, volume, and chemical potential.

Since the work to form a single new surface is γ, the work of cohesion, W_C, of a pure phase is

$$W_C = 2\gamma. \qquad (1)$$

Analogously, in putting two different phases, A and B, in contact, there will be some interaction or adhesion at the interface. The interfacial free energy γ_{AB}, can be defined as:

$$\gamma_{AB} = \gamma_A + \gamma_{AB} - W_{AB}\,, \qquad (2)$$

where the term W_{AB} is the work of adhesion at the interface.

In considering relevant systems, γ_A is the surface energy of a solid polymer, γ_B the surface tension of water, and W_{AB} the polymer/water interfacial interaction term.

Several variables influence surface and interfacial energies of polymers. The chemical nature of the surface, meaning the types of chemical bonds and atoms present on the surface, affect wettability and contact angles. Smith et al. showed that pronounced changes in wetting characteristics of uncrosslinked polybutadiene films result upon controlled surface oxidation[54]. Crystallinity and molecular orientation are factors. Schonhorn and Ryan, upon measuring the wettability of polyethylene single crystals, showed that the different faces of polymer crystallites have markedly different surface energies[82]. An increase in the number of surface groups per unit area, or density, increases surface energy. Roe has shown that the critical surface tension, which has been used as an estimate of surface energy

of polymers, is proportional to the fourth power of the amorphous density for polyethylene[83].

The energy available at a surface in normal atmospheres may serve as a driving force for the reduction of that energy. High surface free energy materials such as metals are often covered with a series of layers, each of which serves to reduce the energy of the surface. An oxide or sulfide may form first, followed by a polar layer such as water vapor. This trend continues until the final surface in a relatively hydrophobic environment such as air, is a low energy, nonpolar organic.

By analogy, the energy available at the interface when a polymer is placed in contact with water in which mobile molecules such as protein are dissolved, may be the driving force behind the eventual interfacial adsorption of protein.

In addition, it is now realized that polymers, due to their weak secondary intermolecular bonds, are relatively mobile, and may reorient in response to a new environment. For example, a polymer with a nonpolar backbone and polar sidegroups may tend to bury the sidegroups in the bulk when in contact with a hydrophobic environment. In contrast, the same polymer in contact with water may reorient polar groups to contact the water phase in an attempt to lower the energy at the interface.

Fowkes proposed that surface energy may be considered to be the sum of terms, each due to a single type of intermolecular force[55]:

$$\gamma = \gamma^{\text{dispersion}} + \gamma^{\text{dipole}} + \gamma^{\text{metallic}} \qquad (3)$$

Where two phases meet, forces of a similar kind operate across the interface, reducing the interfacial free energy, and giving rise to the W_{AB} term of equation (2). The net interfacial energy is then largely due to the extent to which surface forces are not able to operate across the interface, and is a

measure of unsatisfied bonding capacity at the interface. Thus, a very nonpolar polymer such as polyethylene has a low surface energy of 32.4 ergs/cm^2 when in contact with air, while in water the interfacial energy increases to 38.0 ergs/cm^2, due to the inability of polar bonds in water to be completed across the interface. In contrast, the highly polar glass surface has a surface energy of 170 ergs/cm^2 in air, but a low interfacial energy in water of 23.8 ergs/cm^2[84].

A variety of methods are available for the direct measurement of the surface tensions of liquids, such as capillary rise, the DuNouy ring method and pendant drop profiles. Direct measurements are successful due to the ease with which liquids reversibly form new surface.

In contrast, in attempting to measure the surface tension of a solid, stretching the surface does not result in new surface with properties identical to the original. In response to surface tensile forces, atoms in a solid do not move from bulk to surface; they simply separate. For this reason, surface energies of solids can only be determined by indirect means or by estimation.

Solid/liquid interaction terms can also only be estimated, usually by contact angle methods along with assumptions regarding the nature of the components of force operating at the interface.

Surface energies of polymers: The pendant drop method is suitable for measuring surface tensions of viscous liquids. It is a static method, and therefore measurements are not much affected by viscous drag in the liquid. Since density is usually "piece-wise" linear over short temperature ranges with changes in slope at secondary transition points, it is expected that surface tension would behave similarly. Extrapolation of direct measurements to room temperature should give a reasonable estimate of the surface energy of the solid.

Surface tensions of sample polymers as measured by the pendant drop method are shown in Fig. 13. The data show good linearity. The extrapolated value for polystyrene at 20°C, 46.0 ergs/cm^2, is high compared to that found by Wu, 40.7 ergs/cm^2, using a similar method[57]. The density found in this work, 1.08 g/cm^3 at 20°C, Fig. 14, agrees closely with that used by Wu, 1.06 g/cm^3, and with other sources[85].

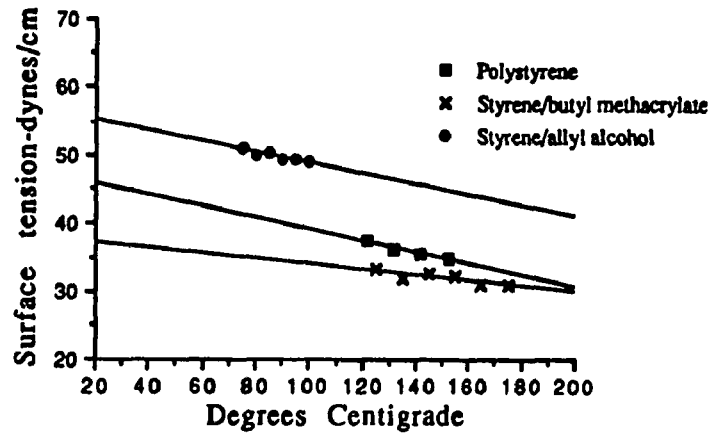

Fig. 13. Surface tensions of polymers as a function of temperature determined by pendant drop method.

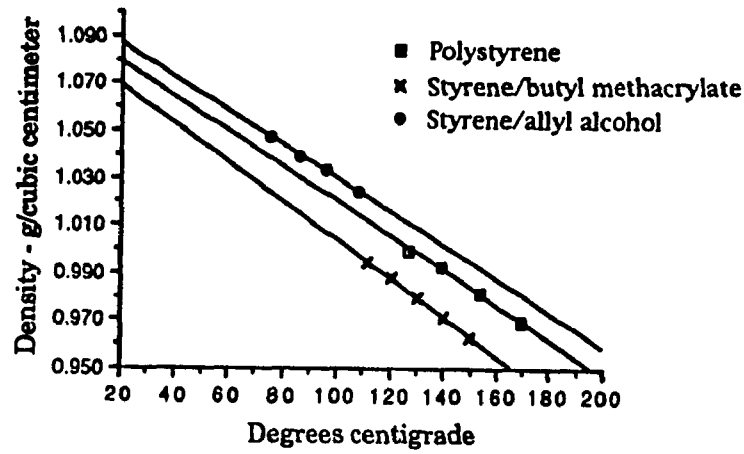

Fig. 14. Polymer densities as a function of temperature.

Other estimates of the surface energy of polystyrene at room temperature include a contact angle method of Owens and Wendt[86], which gave a value of 42.0 ergs/cm^2, a contact angle method used by Wu[87] which gave 42.6 ergs/cm^2, and critical surface tension values, which have been reported for polystyrene by several authors to be 33, 35, 43, and 44 ergs/cm^2 [88,89,90,91].

Room temperature values for the two copolymers were found in this work to be 55.1 ergs/cm^2 for poly(co-styrene-allyl alcohol) and 37.2 ergs/cm^2 for poly(co-styrene-butyl methacrylate). While similar data for the copolymers was not available, the pendant drop method of estimating surface energy has been applied to a wide variety of polymers by several authors. Typical results range from 20 ergs/cm^2 for polydimethylsiloxane to 44 ergs/cm^2 for polychloroprene[91].

Polymer/water interaction terms: In 1964, Fowkes suggested that the dispersion contribution to the interfacial energy could be approximated by a geometric mean relationship of the dispersion components of the two interacting phases[55].

$$W_{12}^{d} = 2\left(\gamma_1^{d}\gamma_2^{d}\right)^{1/2} \qquad (4)$$

Since then, attempts have been made to extend this relationship to the polar component as well. While theoretically it can be shown that under very specific conditions the polar component can be described by a geometric mean, in practice the geometric mean approximation when used with contact angles routinely over or underestimates the contribution from the polar component to the work of adhesion. This is a significant error in polymer/water systems, since, while the dispersion component makes up a significant part of the surface energies, it is largely the disparity in the polar components which determines the interfacial energy. For example, Wu, in direct measurements of the interfacial tension of polystyrene and

polyethylene and of the surface tension of polystyrene by the pendant drop method, found the polar component of polystyrene at 20°C to be 6.8 ergs/cm^2, and a polarity, γ^p/γ, of 0.17[57]. A geometric mean approximation of the polar component of polystyrene from contact angle measurements predicts a very low value of 0.6 ergs/cm^2, or a polarity of 0.02.

The suitability of the geometric mean approximation for the dispersion component is well accepted. The mean can be expressed in terms of London's theory[92]. Polar interactions include dipole-dipole, dipole-induced dipole, and hydrogen bonding interactions among others. The dipole interactions have been expressed in terms of the Debye-Keesom theories[57]. However, no satisfactory expression describing hydrogen bonding interactions is available.

Recently, Fowkes began developing means to estimate the polar contribution to the interfacial energy using a partial acid-base approach. Recent evidence has suggested that the extrapolation of the dipole interactions of the Debye-Keesom theories from gases to condensed phases may not be valid[93].

A harmonic mean relationship appears to be an improvement on the geometric mean. Using the assumption of identical polarizabilities of the interacting phases rather than identical vibrational frequencies as assumed by Fowkes, Wu developed the harmonic mean relationship for the dispersion component, and then extended it to the polar component as well[57]:

$$W_{12} = -\frac{4\gamma_1^d\gamma_2^d}{\gamma_1^d + \gamma_2^d} - \frac{4\gamma_1^p\gamma_2^p}{\gamma_1^p + \gamma_2^p} \qquad (5)$$

From contact angles, this equation predicts a still low polar component for polystyrene of 4.3 ergs/cm^2, and a polarity of 0.10[87].

Results from this work using the harmonic mean relationship and contact angles of water and methylene iodide to estimate polar and dispersion components of the sample polymers are shown in Table 1. The procedure is outlined in Appendix B. The components and polarity for polystyrene show good agreement to those found by Wu, using the same method[87]. Comparable data could not be found for the copolymers.

	Contact angle-degrees		ergs/cm^2			
Surface	Water	Methylene Iodide	γ^d	γ^p	γ	γ^p/γ
Polystyrene	90.3±0.8	38.3±1.8	38.2	4.6	42.8	0.11
Styrene/butyl methacrylate	86.5±1.9	55.3±2.9	30.4	7.6	38.0	0.20
Styrene/allyl alcohol	80.5±1.5	29.8±1.5	41.5	8.9	50.4	0.18

Table 1. Surface and component energies for sample polymers from contact angles and harmonic mean approximation.

Of the three materials, this method predicts the highest polarity for poly(co-styrene-butyl methacrylate). From the lower water contact angle and from Wilhelmy plate studies to be discussed, it is expected that the highest polarity should belong to poly(co-styrene-allyl alcohol). That this method does not predict it may be due to inaccurate estimation of the polar component.

An alternative method for obtaining the polar and dispersion components of the sample polymers for use in the harmonic mean relationship is the following. Contact angles on the solid are made using a liquid whose only interactions are dispersion. The dispersion component of the solid can then be directly determined using a geometric mean approximation, an appropriate

assumption. The polar component is then the difference from surface energies determined from pendant drops. Methylene iodide has a very low, 1.3 ergs/cm^2[87], or zero[93] polar component and a high surface tension, 58.0 ergs/cm^2. Using this method, the largest polarity was predicted for poly(co-styrene-allyl alcohol), Table 2.

	Contact angle-degrees	ergs/cm^2			
Surface	Methylene Iodide	γ^d	γ^p	γ	γ^p/γ
Polystyrene	38.3±1.8	41.0	5.0	46.0	0.11
Styrene/butyl methacrylate	55.3±2.9	32.1	5.1	37.2	0.14
Styrene/allyl alcohol	29.8±1.5	45.5	9.6	55.1	0.17

Table 2. Surface and component energies for sample polymers from geometric mean approximation and pendant drop results.

Interfacial energies: Interfacial energies using the two methods are shown in Table 3. In either case, the sample materials provided only a very narrow range of interfacial properties. Interfacial energies in mercury/organic liquid systems are as high as 390 ergs/cm^2.

Surface	Method 1*	Method 2+
Polystyrene	46.4	43.7 ergs/cm^2
Styrene/butyl methacrylate	32.5	39.5
Styrene/allyl alcohol	40.3	36.6

Table 3. Interfacial energies. * γ^d and γ^p determined from harmonic mean equation. + γ^d and γ^p determined from geometric mean equation and pendant drop results.

Equilibrium conditions were assumed in the above procedures. Contact angles were measured within 15 seconds of drop placement. The time-dependent nature of the sample surfaces in a water environment is verified by the Wilhelmy plate study which follows.

Wilhelmy plate

A liquid drop takes on the shape which minimizes the free energy of the system. In the absence of gravity, this is equivalent to minimizing the surface area of the drop. At equilibrium, the drop which results is spherical. Upon contact with a solid surface, the drop again takes the shape which minimizes the free energy of the system. Gibbs showed that minimizing this free energy required the minimization of[94]:

$$\gamma_{lg}A_{lg} + \gamma_{sg}A_{sg} + \gamma_{sl}A_{sl} \ , \qquad (6)$$

where γ is a surface or interfacial tension, A an area, and the subscripts lg, sg and sl refer to liquid-gas, solid-gas and solid-liquid interfaces.

For a plane, homogeneous, nondeformable surface, the minimization yields[94]:

$$\gamma_{lg}\cos\theta = \gamma_{sg} - \gamma_{sl} \ , \qquad (7)$$

where θ is the contact angle. This equation is known as Young's equation, after Thomas Young.

The angle that the liquid makes with the solid is the result of a balance between cohesive forces in the liquid and adhesive forces between the solid and the liquid. If there were no interaction between solid and liquid, the solid-liquid surface tension would be equal to the sum of γ_{sg} and γ_{lg}, and the contact

angle would be 180°. Due to interactions, the liquid spreads until equation (7) is satisfied.

For the above idealized situation, a liquid drop on a plane, homogeneous, nondeformable surface, there will be only one equilibrium thermodynamically stable contact angle. However, this is rarely the case.

The following situations contribute to nonideality, and complicate the interpretation of contact angle measurements[69]:

1) a deformable solid surface (With water, this factor is relevant when the modulus of elasticity is less than 3.5×10^5 dynes/cm^2.),

2) a rough surface (This effect appears to be significant for surfaces that are not smooth at the 0.1mm level.),

3) a nonhomogeneous surface (Block copolymers or polymer blends or dirt on the surface will very likely result in patches of different surface energies.),

4) a probe liquid whose surface tension changes during the course of the measurement (This is commonly due to the extraction of low molecular weight components from the solid.),

5) solid and liquid phases which interact in ways other than the three-phase equilibrium noted earlier (An example would be swelling of the solid surface.), and

6) groups at or near the surface of the solid which are able to change their configurations in response to a new environment.

The presence of one or more of the above situations results in contact angle hysteresis. Hysteresis refers to the difference in the contact angle measured upon advancing a liquid over the surface compared to that upon retracting the liquid over the surface.

Two classes of hysteresis are recognized[69]:

1) True or thermodynamic hysteresis. The hysteresis is reproducible over many cycles and is not time or frequency dependent. Conditions giving rise to true hysteresis include surface roughness and surface heterogeneity.

2) Kinetic hysteresis. The hysteresis is time or frequency dependent, and is generally due to slow equilibrium times. Deformable surfaces, surface swelling induced by solvent penetration, and reorientation and mobility of groups near the surface all give rise to hysteresis of this type.

Fig. 15 shows a curve obtained when an acid-cleaned oxide-covered silicon wafer with no polymer layer is tested using the Wilhelmy plate method. No hysteresis is seen. This result verifies the adequacy of the wafer cleaning procedure, and indicates that the wafers, highly polished on both sides, have no roughness detectable by the test method. Upon addition of thin (order of nanometers) polymer layers, the wafer appearance remained unchanged. This indicates that thin polymer layers were smooth at the 0.1mm level, and that roughness contributed little or nothing to hysteresis. The addition of thick (order of micrometers) layers did noticeably change wafer appearance. Roughness, which generally contributes only a few degrees to hysteresis[69], may have been a factor in these samples.

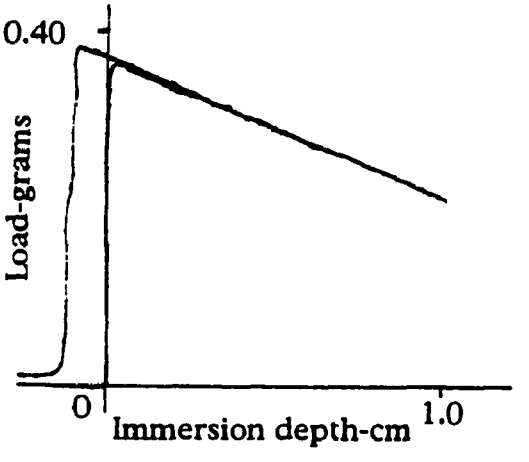

Fig. 15. Wilhelmy hysteresis loop obtained from acid-cleaned, oxide-covered silicon wafer.

It is unlikely that the surfaces were deformable. Polystyrene has a relatively high elastic modulus of 2.8×10^{10} dynes/cm^2[85].

Thick (micrometers) polymer samples: A significant hysteresis and continued change in both advancing and receding contact angles was noted for each material for the 30 hour duration of the test, Fig. 16. The continued change indicates that hysteresis was of the kinetic type. Possible causes of change include water penetration of the surface and/or reorientation of groups at the surface. The driving force for reorientation of surface groups is the minimization of interfacial free energy.

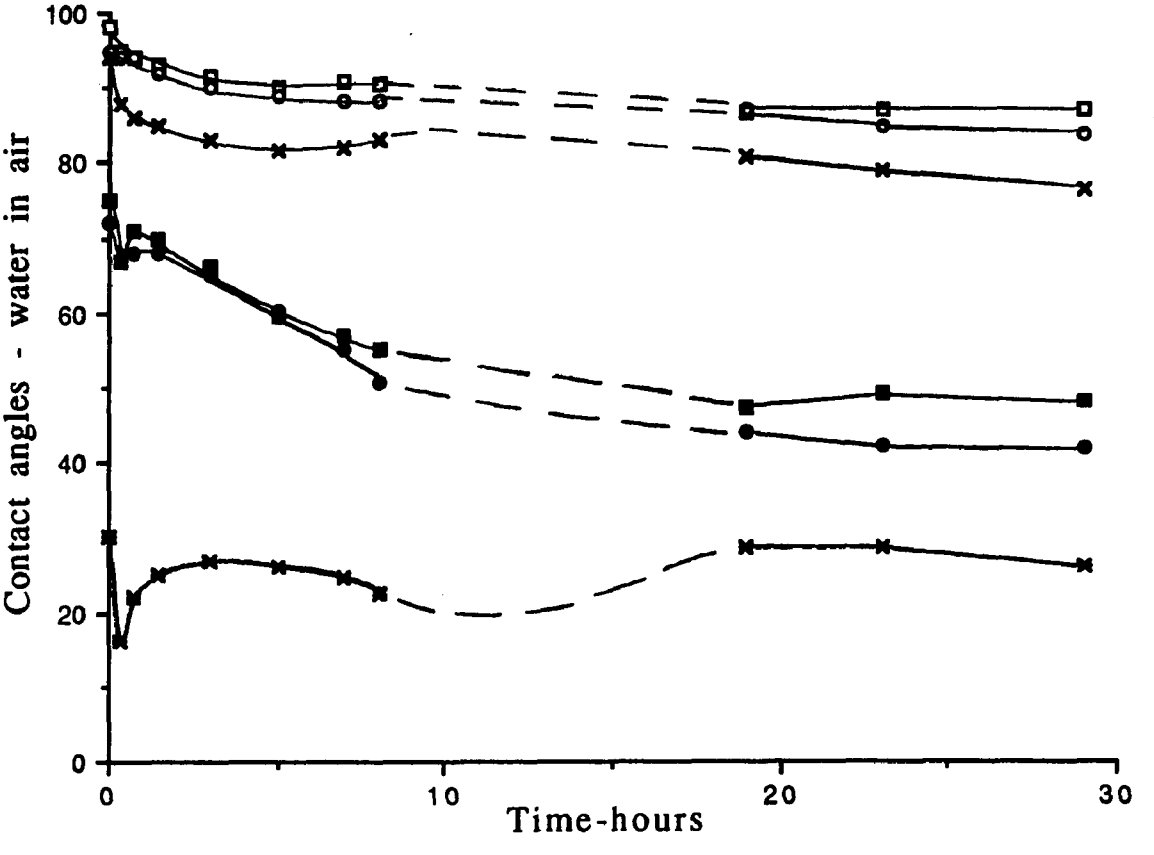

Fig. 16. Contact angles vs immersion time in water from Wilhelmy plate results on thick samples.

- □ Polystyrene-Advancing angles
- ■ Polystyrene-Receding angles
- ○ Styrene/butyl methacrylate-Advancing angles
- ● Styrene/butyl methacrylate-Receding angles
- × Styrene/allyl alcohol-Advancing angles
- ✖ Styrene/allyl alcohol-Receding angles

Water penetration and plasticization of the region near the surface is not unlikely, despite the hydrophobic nature of the sample. The molecular volume of water, 18 ml/g·mole, is low. In turn, plasticization would promote motions of chain segments and side groups. Reorientation of polar groups or segments toward the water phase would result in a more wettable surface with time, reducing the contact angle. The low receding angles of poly(co-styrene-allyl alcohol) sample may be an example. The first specimen tested was dry. During the course of the test, sample/water contact time was about two minutes. This may have been enough time for water to be attracted to surface hydroxyl groups, plasticize the surface, and allow the reorientation of additional hydroxyl groups toward the interface.

Pronounced fluctuations were noted in the receding curves. Johnson and Dettre, from studies of a series of two-phase materials of varying surface composition, noted that advancing angles remained high despite a surface composition of over 95% wettable phase[95]. Receding angles, however, decreased considerably with the introduction into the surface of just 5% wettable phase. These results suggest that molecular motions which result in a more wettable surface will produce pronounced changes in receding curves.

A plasticized surface is likely to be heterogeneous with respect to surface energies. Some hysteresis noted may have been due to this effect.

The difference between advancing and receding angles at 30 hours was 40° for polystyrene and poly(co-styrene-butyl methacrylate), and 50° for poly(co-styrene-allyl alcohol). Holly and Refojo found hysteresis ranging from 40° to 75° for a series of poly(hydroxyethyl methacrylate) polymers using sessile drop and captive air bubble methods[48]. Hysteresis using the Wilhelmy plate method was found by Smith to range from 35° to 50° for polybutadiene films of

controlled surface characteristics[54]. Good and Kotsidas found a hysteresis of 26° using a sessile bubble technique with crosslinked polystyrene[51].

Thin (nanometers) polymer samples: Results for wafers with thin polymer layers are qualitatively similar, Fig. 17. Hysteresis was kinetic, and of similar magnitude. Changes in receding angles were again pronounced. This result suggests that plasticization and/or mobility occurred as readily in thin as in thick samples.

As testing time approached 30 hours, changes in the curves slowed. From these results, and for the remainder of this work, water contact time of 48 hours was assumed to be sufficient for sample equilibration.

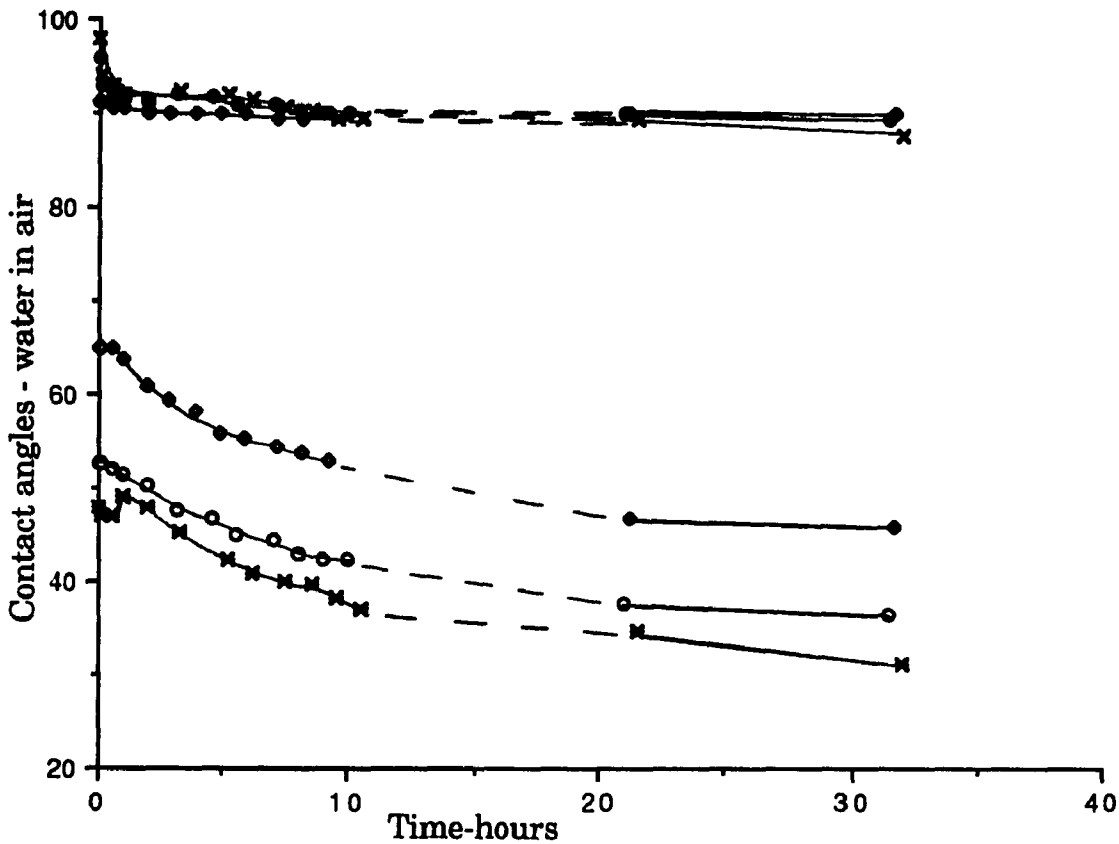

Fig. 17. Contact angles vs immersion time in water from Wilhelmy plate results on thin samples.

- ● Polystyrene-Advancing angles
- ● Styrene/butyl methacrylate-Advancing angles
- × Styrene/allyl alcohol-Advancing angles
- ● Polystyrene-Receding angles
- o Styrene/butyl methacrylate-Receding angles
- ✖ Styrene/allyl alcohol-Receding angles

Microcalorimetry

Protein molecules are copolymers of about 22 amino acids linked to each other by polycondensation, forming a polypeptide chain. The amino acid sequence within the chain is known as the primary structure of the protein. Within each peptide unit, two of the three bonds are free to rotate. The C-N bond, due to its partial double bond character, is fixed. Peptide side groups are positioned in the trans configuration to minimize steric hindrance. Due to the acidic or basic nature of some side groups, and their varying hydrophobicities, polypeptide chains are often amphoteric, amphiphilic molecules.

Secondary structure describes the repetitive spatial organization of the chain backbone. Common conformations include the α-helix and the β-sheet, which comprise 40-70% of most globular proteins, and random coil. The formation of α-helix and β-sheet results in a decrease in rotational mobility of chain residues and a decrease in conformational entropy. The resulting decrease in the $T\Delta S$ term typically causes an increase in G on the order of a few hundreds kJ/mole for a protein of molecular weight 10,000[96]. In general, α-helix and β-sheet structures are stabilized by the formation of hydrogen bonds between residues.

Tertiary structure describes the spatial folding of the chain. The major driving force for folding a chain into a compact structure is the dehydration of hydrophobic side groups. Contacts between water molecules are much more favorable energetically than are contacts between non-polar groups or between a non-polar group and water. As non-polar side groups are rejected from an aqueous environment, a large increase in the entropy of water results as it is released from non-polar contacts. It has been estimated that the contribution from hydrophobic dehydration toward reducing ΔG is about

500 kJ/mole for a typical globular protein of molecular weight 10,000[96].

Rotational freedom and hydrophobic dehydration are the major forces determining protein stability. Smaller factors include coulombic interactions, which promote less stable expanded structures away from the isoelectric point of the protein, and dipolar and dispersion interactions, which favor a compact structure.

As a result, globular proteins in an aqueous environment tend to be roughly spherical with a packing density of 0.70-0.80. Polar and charged groups tend to be situated at the molecule's exterior, while non-polar side groups tend to be buried in the interior.

In large part, one contribution to ΔG is offset by another, and the native protein in aqueous solution is only very marginally thermodynamically stable. Even subtle changes in the microenvironment of the molecule such as temperature, pH, and ionic strength can induce a change in conformational state. From a series of studies employing a variety of denaturing conditions, it was concluded that the free energy change in going from the native to an available denatured state is only about 10 kcal/mole for a typical globular protein of molecular weight 15,000[97].

In addition, internal energy fluctuations within the molecule amount to about 40 kcal/mole in a protein of molecular weight 25,000[98], suggesting that a spectrum of conformational states may exist simultaneously, and that conformational mobility must be expected.

It has been established from *in vitro* folding and denaturation studies that conformational changes of various types occur in the time span 0.1 to 100 seconds[99]. It is thought that stable domains within the structure, such as α-helix, provide a nucleus for additional folding or organization.

However, despite the dynamic nature of the protein molecule, internal constraints are apparently large enough that gross deviation from the compact structure observed crystallographically does not occur[98].

From systematic studies of the adsorption of well-characterized model proteins by various well-defined surfaces, a few trends are apparent[39-42, 100]. For proteins with high structural stability, as may be determined by the Gibbs energy of denaturation, adsorption is governed primarily by electrostatic interactions between protein and surface, and somewhat by hydrophobic dehydration of the surfaces of the substrate and the protein. While conformational changes within the protein may occur, strong internal coherence keeps them to a minimum. On the other hand, proteins with low structural stability may adsorb with pronounced structural rearrangement, often despite electrostatic repulsion between surface and protein. The large entropy gain due to loss of secondary structure, along with entropy gained as non-polar parts of the protein interior contact hydrophobic patches on the substrate surface, provides the thermodynamic advantage allowing adsorption.

Thus, major subprocesses involved in protein adsorption include changes in the state of hydration of the substrate and protein surfaces, rearrangements within the protein structure, as well as movement of ions into and out from the adsorbed layer. Each subprocess contributes an entropy and an enthalpy to the overall adsorption process:

$$\Delta_{ads}G = \Delta_{ads}H - T\Delta_{ads}S \qquad (28)$$

where G is the Gibbs free energy, and H, S and T refer to the enthalpy, entropy and absolute temperature. For the process to occur spontaneously, ΔG must be negative.

Protein adsorption is not a completely reversible process and cannot be treated as such. Exposure of the adsorbed protein to pure solvent does not generally lead to desorption in reasonable times. Langmuir theory, and its assumptions of reversibility as well as the absence of lateral interactions, is therefore not valid. A direct statistical analysis of $\Delta_{ads}S$ is impractical due to the large number of protein and solvent changes during adsorption. This leaves $\Delta_{ads}H$, which, under constant pressure conditions, is equal to the heat of adsorption, and can be measured in a microcalorimeter.

Microcalorimetric heats are the sum of heats generated by each subprocess. Using a semi-quantitative approach, Norde and Lyklema[101] resolved the integral adsorption heat into its components for the adsorption of human plasma albumin and ribonuclease, two very different proteins with regard to structural stability and isoelectric point, onto negatively charged polystyrene, Fig. 18. From dissolution heats of ethylbenzene in water, they concluded that hydrophobic dehydration of substrate and protein surfaces generates small exothermic heats. The contribution from overlapping of substrate and protein electric fields was determined from calculation to be small and endothermic. From titration data before and after adsorption, the transfer of ions into and out from the adsorbed layer in response to the electric field of the charged surface was in both cases determined to be large and exothermic. Upon subtracting these heats from the measured integral adsorption heat, they were able to conclude that the heat associated with structural rearrangement upon adsorption is large and endothermic. The overall integral heat was either exothermic or endothermic depending upon the relative magnitudes of the components, and appeared to be a strong function of pH.

Hen egg lysozyme, a small (MW 14,400, 3.0x3.0x4.5nm[102]) globular enzyme with antibacterial activity has a Gibbs energy of denaturation of 4.1 J/g[103],

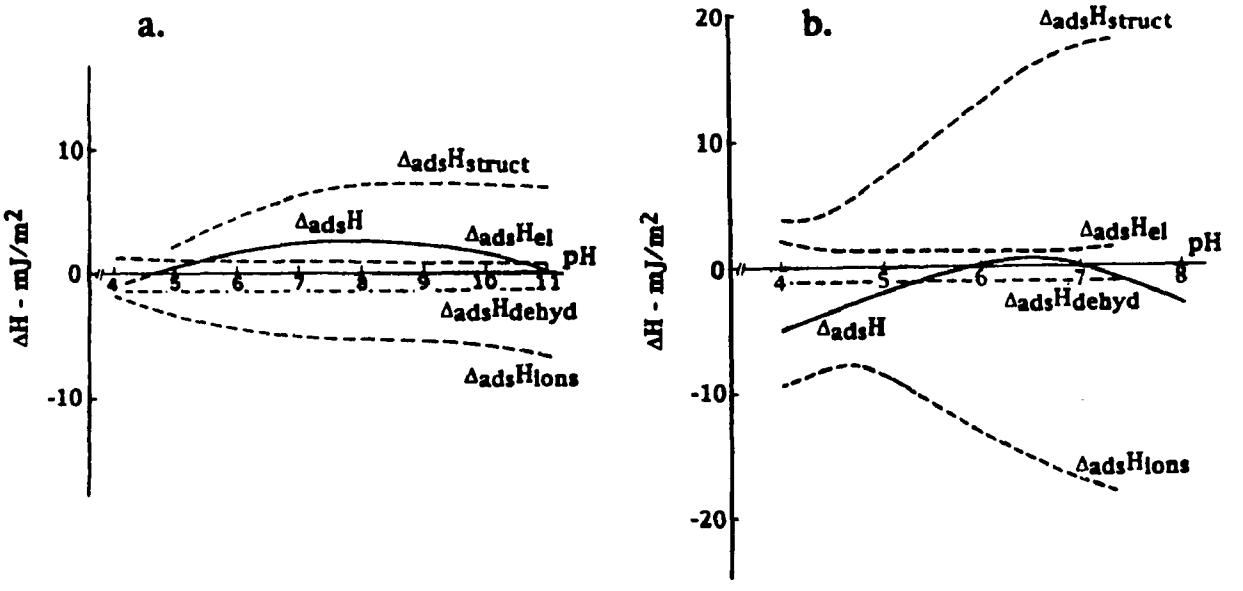

Fig. 18. Resolution of the integral heat of adsorption of: a. Bovine pancreas ribonuclease, and b. Human serum albumin into its components. Substrate - negatively charged polystyrene. Struct.=structural rearrangement, El.=overlap of electric fields, Dehyd.=dehydration of protein and substrate, Ions=ion transfer. (Adapted from Norde and Lyklema, 1979)

making it fairly rigid with respect to similar proteins. Lysozyme consists of 40% α-helix and 12% β-sheet[102] and has an average overall hydrophobicity[104]. Under the experimental conditions of this work, the molecule had a net positive charge (isoelectric point 11.1). This protein was chosen because it has been thoroughly characterized, and because it is globular as are relevant blood proteins.

The three substrates were chosen to provide a range of interfacial characteristics. At pH 7.14, no ionizable groups were present on any of the three. The varying polarities likely resulted in different densities of associated ions at the interfaces, but it is expected that the electric field associated with each interface was small.

From the adsorption isotherm and integral adsorption heats for polystyrene, ionic strength 0.1M, Fig. 19, two trends are apparent. As bulk lysozyme concentration increased, the amount of lysozyme adsorbed by substrate followed a step pattern, with a series of plateaus showing successively higher adsorbed amounts. In addition, adsorption heats showed endothermic discontinuities at each rise between plateaus. Heats at other points, including those at zero protein concentration, were exothermic and apparently due to dilution of buffer ions by pure water in the sample holder.

Similar step patterns are seen in Figs. 20 and 21 for the other two polymers. In the case of poly(co-styrene-butyl methacrylate) substrate, endothermic discontinuities again occurred at rises between plateaus. With poly(co-styrene-allyl alcohol) substrate, no discontinuities were found, and all heats were of the magnitude of dilution heats.

These three figures suggest that while adsorption occurred readily, the only detectable heats possibly related to adsorption occurred at rises between plateaus. Elsewhere, measured heats were negligible. Norde and Lyklema[101] found the integral heat to be small or zero at particular pH values depending upon the relative magnitudes of the components. At plateaus in Figs. 19-21, negligible heats found there likely reflect compensating subprocess reactions.

A non-zero heat associated with structural rearrangement upon adsorption is suggested by FTIR results shown in Fig. 22. The amide I band at 1660 cm^{-1} is attributable predominantly to C=O stretching in α-helix, and the amide II band at 1540 cm^{-1} predominantly to N-H deformation in α-helix[105]. Their relative intensities changed considerably upon adsorption, strongly suggesting structural rearrangement. Norde and Lyklema found the heat associated with structural rearrangement to be 7 mJ/m^2 for ribonuclease, a protein with structural stability similar to that of lysozyme, $\Delta G_{denat.}$= -3.6 J/g[103]. A heat of

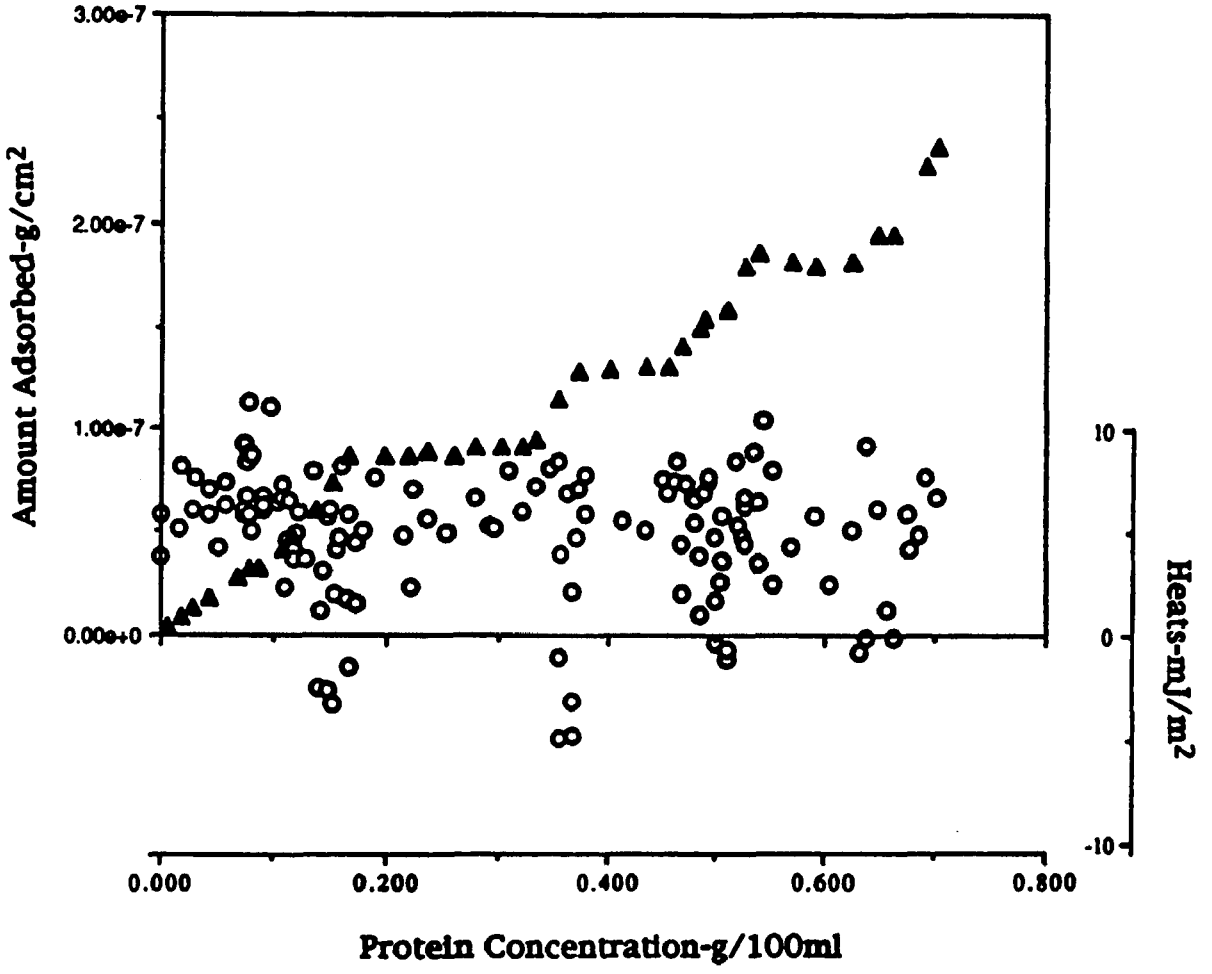

Fig. 19. Adsorption isotherm (▲) and microcalorimetric heats (O) for polystyrene at ionic strength of 0.1M from phosphate buffer.

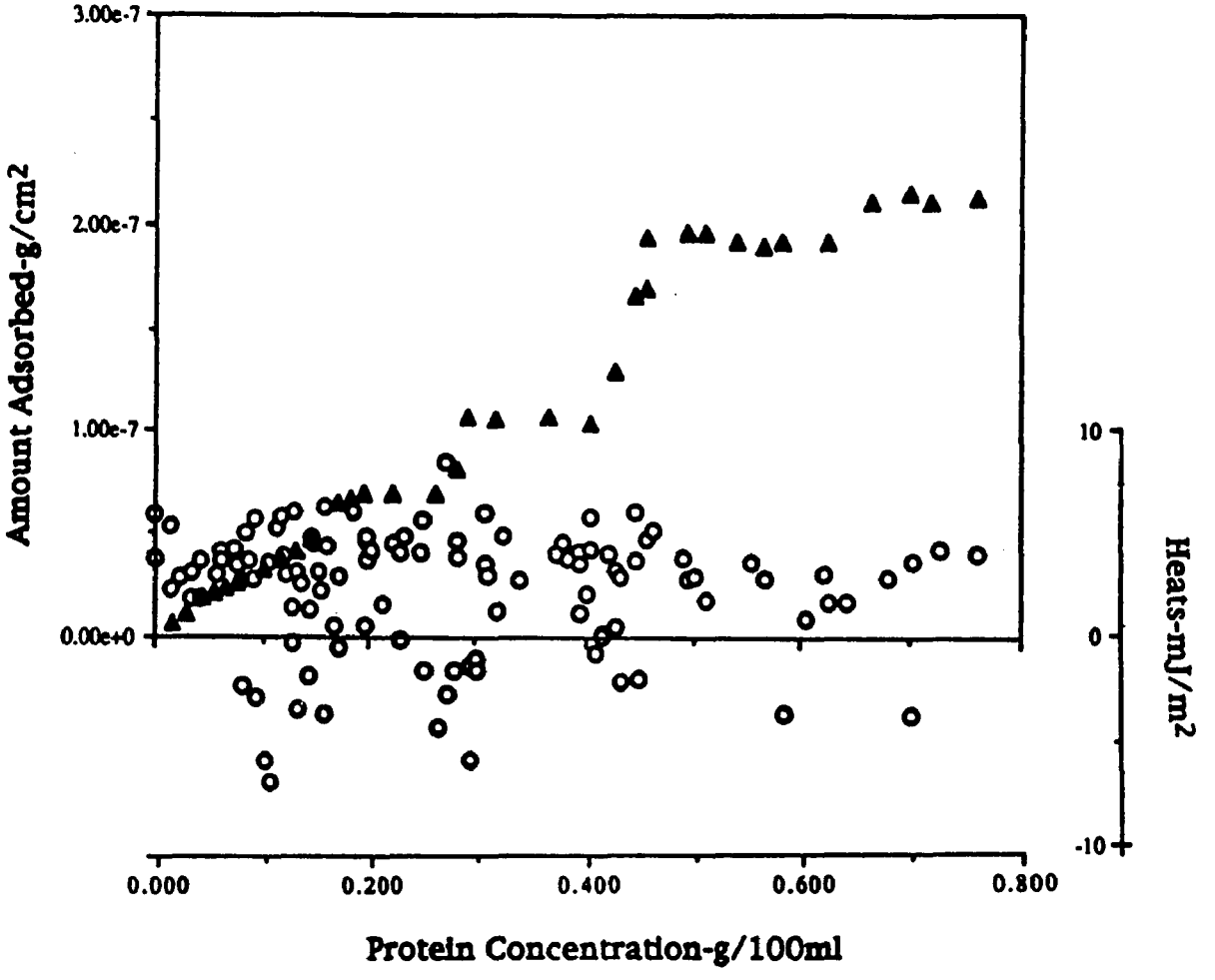

Fig. 20. Adsorption isotherm (▲) and microcalorimetric heats (O) for styrene/butyl methacrylate at ionic strength of 0.1M from phosphate buffer.

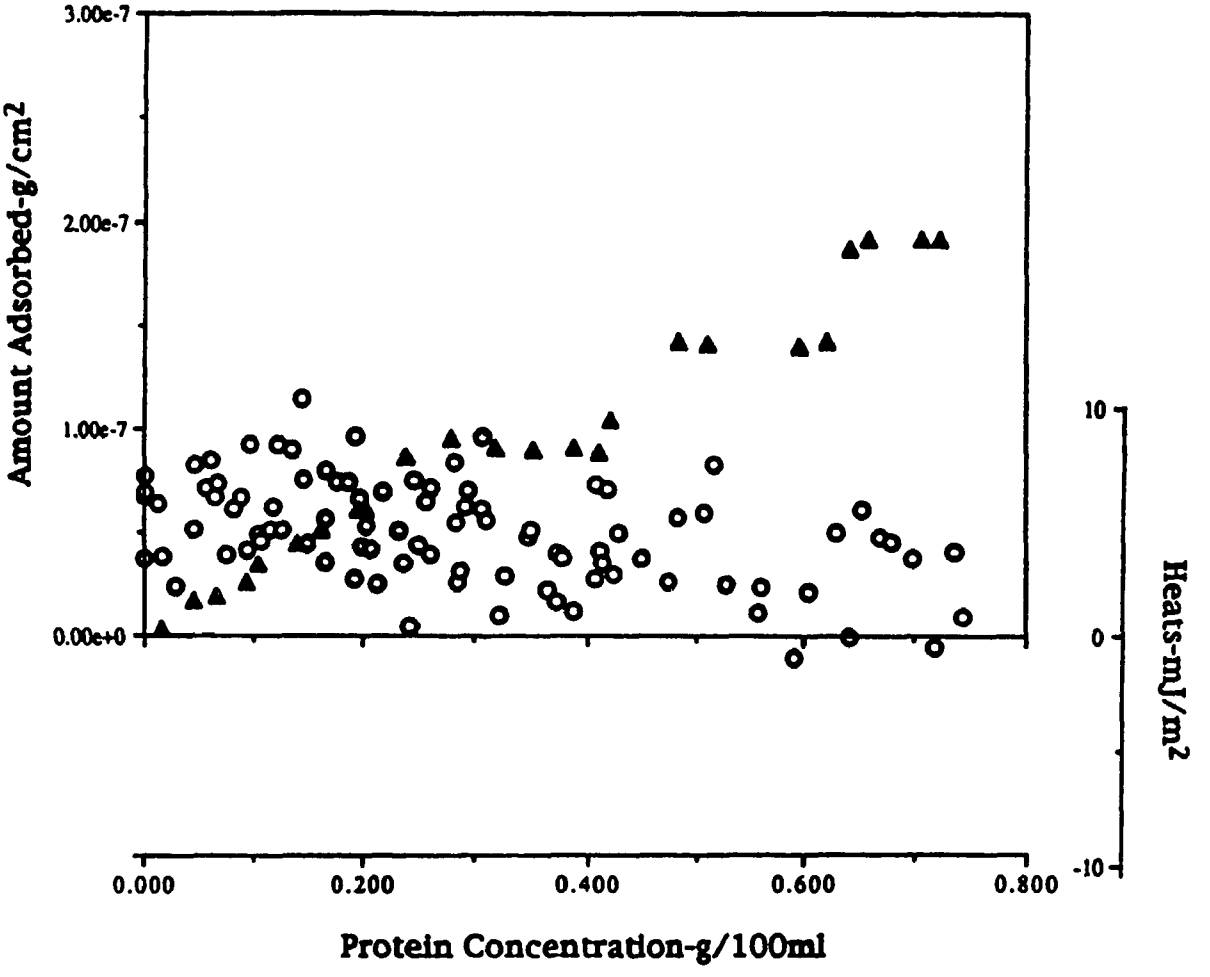

Fig. 21. Adsorption isotherm (▲) and microcalorimetric heats (O) for styrene/allyl alcohol at ionic strength of 0.1M from phosphate buffer.

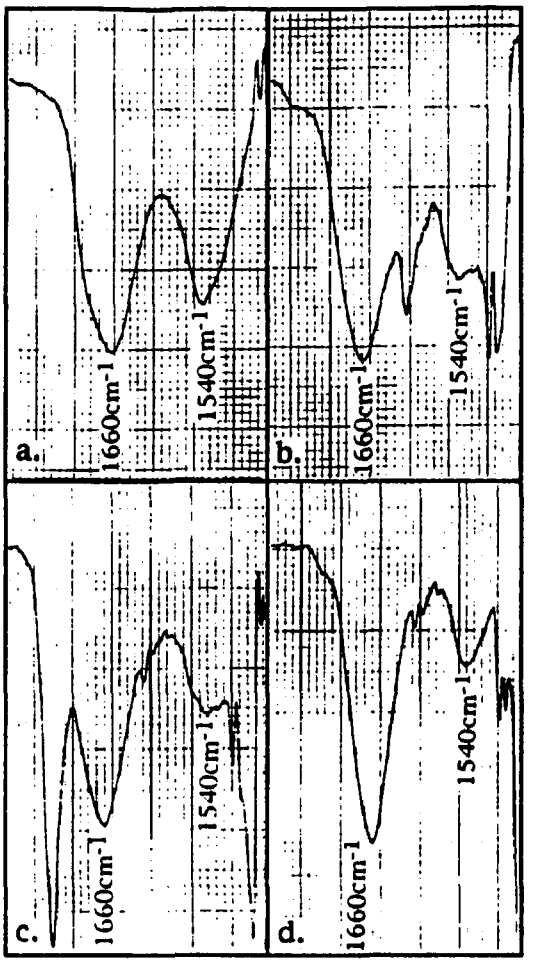

Fig. 22. FTIR spectra of amide I and II bands:
a. Bulk lysozyme, I/II=1.36,
b. Polystyrene/lysozyme, I/II=1.42,
c. Styrene/butyl methacrylate/lysozyme, I/II=1.76, and
d. Styrene/allyl alcohol/lysozyme, I/II=2.56.

this magnitude is easily detectable by the experimental apparatus used in this work.

The non-high affinity isotherm is typical of compact molecules like globular proteins. These molecules attempt to attach via several contacts to the substrate surface. Since they are not as flexible as homopolymers, their free energy of adsorption is smaller and is reflected in the shape of the adsorption isotherm. A finite initial slope results.

A second feature commonly seen with compact molecules is a well-defined plateau. A plateau is generally considered to represent saturation of the

surface by an adsorbing species, forming a monolayer. Saturation is suggested by the uniformity of amount adsorbed despite an increase in pressure or concentration. The maximum number of molecules which the surface can accommodate is assumed to be limited at least in part by crowding or by charge repulsion. The latter is suggested by studies which show plateau adsorption to be a maximum at the isoelectric point of a protein, with smaller values elsewhere[100].

Isotherms with two plateaus have been reported. Fair and Jamieson have proposed a bimodal mechanism for the adsorption of bovine albumin by polystyrene latex which causes three regimes of structure[29]. At lower concentrations, they propose that molecules adsorb in a random, independent way, giving rise to the first plateau. At high concentrations, intermolecular nucleation at the sorbent surface results in the formation of a two-dimensional protein crystal. The transition region between the two plateaus consists of an unordered, glassy structure. From their data, the first plateau corresponds to a surface concentration of 1.3 molecules/100nm^2, or a surface coverage of 69% if the molecules adsorb "side-on" and no spreading is assumed. The second plateau corresponds to a concentration of 2.3 molecules/100nm^2.

Multiple plateaus have been reported. Hlady found the adsorption of human serum albumin by hydroxyapatite to show multiple steps over a wide range of pH values[30]. He found initial plateaus to correspond to a range of surface concentrations, from 1.3 molecules/100nm^2 at pH values near the isoelectric point of albumin, to 0.2 molecules/100nm^2 at pH values far from the isoelectric point. Final plateau concentrations ranged from 2.8 molecules/100nm^2 to 0.3 molecules/100nm^2. Hlady proposed that the plateaus represent distinct protein conformational states.

Chattoraj and Bull, using microelectrophoresis techniques, noted that bovine serum and egg albumin may exist in different conformational states with different numbers of anchoring sites depending upon the pH and protein concentration[31]. They proposed that the protein may initially adsorb as a spread monolayer, then undergo transition to a condensed, perhaps crystalline, state.

Levine has proposed that the adsorption isotherm may reflect surface transitions as characteristic changes in slope[106]. He reasons that equilibrium implies equal activities among the initially adsorbed expanded phase, a condensed transformed phase, and the protein in solution. Assuming that the condensed phase maintains a constant surface concentration, the concentration of protein in all three phases must remain constant as the condensed phase forms at the expense of the expanded phase. The result is an isotherm such as shown in Fig 23. In the region OA, the amount adsorbed increases with amount of protein added. At point A, condensed surface phase II begins to form, and is signaled by a change in slope of the adsorbed amount as well as no change in the concentration remaining in solution. This situation continues until all of phase I is converted to phase II, point B. The expression describing the adsorbed amount between points A and B is:

$$\text{Amount adsorbed} = S\rho_{II}\theta_{II} + S\rho_{I}(1-\theta_{II}) \ , \qquad (9)$$

where S is a surface area, ρ_{I} and ρ_{II} are protein surface concentrations, and θ_{II} the fraction of the surface occupied by phase II. Beyond point B, a plateau representing saturation by phase II is expected.

Similar curves obtained from the early portion of the isotherm of Fig. 19 are shown in Fig. 24. The concentration of protein remaining in solution during transition did not remain constant, but a decrease in slope is noted between

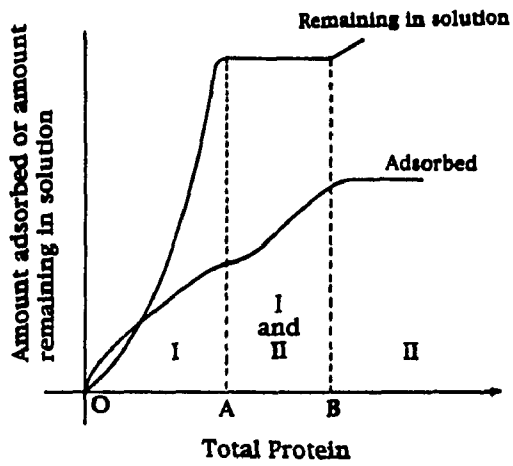

Fig. 23. Schematic drawings of adsorption isotherm and concentration of protein remaining in solution.
I = expanded protein phase, II = condensed protein phase.
(Adapted from Levine, 1969).

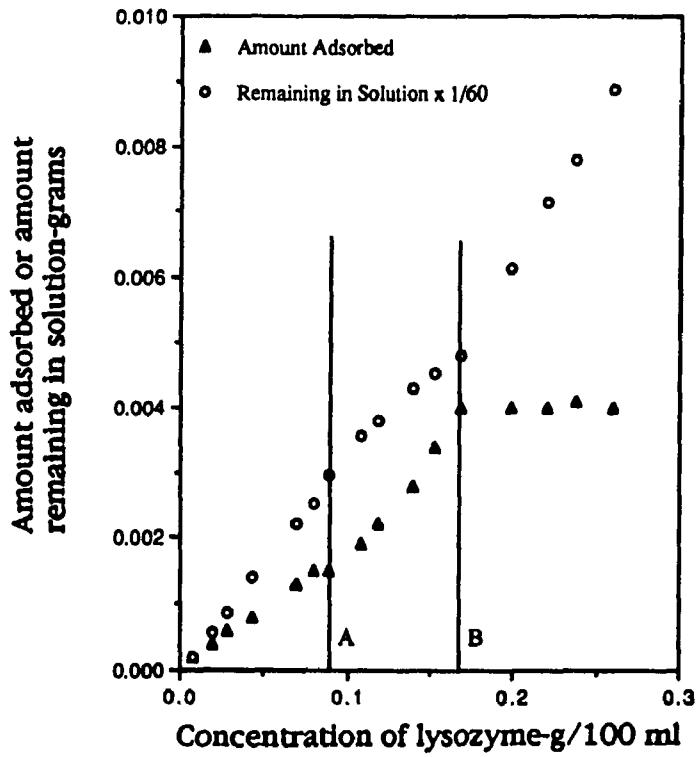

Fig. 24. Adsorption isotherm and concentration of lysozyme remaining in solution for polystyrene at ionic strenth 0.1M from phosphate buffer.

points A and B. Under the experimental conditions of this work, constancy between A and B was not possible because of the very small difference in adsorbed amounts between plateaus relative to the large amount of protein available.

However, the shape of the adsorption curve in Fig. 24 is consistent with the gradual formation of a condensed second phase beginning at point A. The gradual increase in slope past point A indicates a continual increase in average surface protein concentration. This result, along with the formation of a plateau at point B, is consistent with Levine's proposal of the occurrence of multiple surface states, as well as the coexistence of two phases during transition.

Endothermic discontinuities present at each rise between plateaus may correspond to latent heats associated with transitions. This proposal is supported by their absence along the initial ascending portion of the isotherms. Endothermic heats during spontaneous adsorption indicate gains in entropy, most likely due to structural rearrangement. Their magnitudes in Figs. 19 and 20, 7-12 mJ/m^2, agree well with the 7 mJ/m^2 discerned by Norde and Lyklema[101] to be the contribution from structural rearrangement to the integral heat of adsorption of ribonuclease.

The recorded pattern of heats raises a question about starting conditions which led to plateau formation. Enthalpy is a state function and its value does not depend upon a particular reaction pathway. If plateaus represent distinct surface conformations, and if system conditions before adsorption at points A, B and C were identical, recorded enthalpies should look like those in Fig. 25. That is, identical starting conditions at points A, B and C would make pathway (5) —> (6) identical to pathways (1) —> (6) and (3) —> (6). Heats associated with transitions (2) —> (4) and (4) —> (6) must be included in pathway (5) —> (6).

However, starting conditions at points A, B and C were not identical since the system at those points did not behave in the same way; different amounts of protein were adsorbed. Recorded heats generated by transitions need not follow the pattern shown.

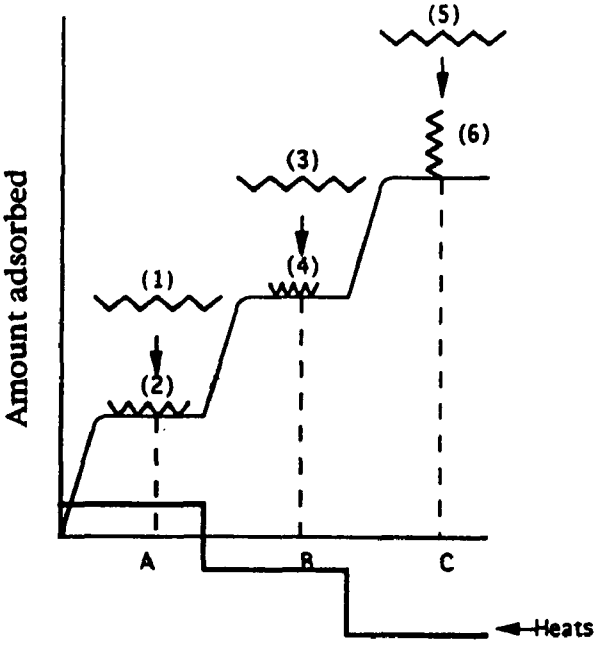

Fig. 25. Schematic drawing of protein conformations and resulting heats assuming identical starting conditions at points A, B and C.

Distinct plateaus, as seen in Figs. 19-21, likely do not represent multiple layers. Protein in solution begins to segregate onto an exposed surface at very low solution concentrations, increasing in amount up to the point of surface saturation, whereupon a new surface is exposed to the solution. An incremental increase in solution concentration would allow segregation at the new surface, and would likely be seen as a decrease in slope in the isotherm reflecting a lower affinity for the new surface.

Plateau values found in this work correspond to far less than one monolayer of packed molecules. In Fig. 19-21, initial plateaus correspond to

surface concentrations of about 1.3 molecules/100nm^2, or a surface coverage of 18% if the molecules adsorbed "side-on" without spreading. The low surface concentration may partly reflect repulsion due to the high positive charge density on the molecule, which at pH 7.14 is far from its isoelectric point.

The low initial surface concentration may also reflect spreading. As adsorption begins, the arrival of molecules at the surface is diffusion-controlled. At low concentrations, an adsorbing molecule has time to increase its surface contacts by spreading before being influenced by an arriving neighbor. The surface can be saturated by few molecules. At high concentrations, the large number of arrivals over a short time prevents extensive surface contact, but permits a higher surface concentration.

In Figs. 19-20, heats per transforming molecule become progressively smaller at successive transitions. If latent heats are directly associated with structural rearrangement, this result implies smaller conformational change with each transition.

The more complete isotherms of Figs. 26-28, ionic strength 0.002M, again likely reflect series of conformational transitions of varying magnitudes. Final plateaus, at concentrations of 1.5%, correspond to surface coverages of 85% if assuming "side-on" attachment, and 57% if the molecules adsorbed "end-on".

The pattern of heats at the lower concentrations of Figs. 26-28 is qualitatively similar but not as clear as are those of Figs. 19-21. Endothermic heats are present in the cases of polystyrene and poly(co-styrene-butyl methacrylate), but largely absent with poly(co-styrene-allyl alcohol). Dilution heats are of smaller magnitude reflecting the lower ionic strength. No pattern of heats is present at higher concentrations. A reason is not clear.

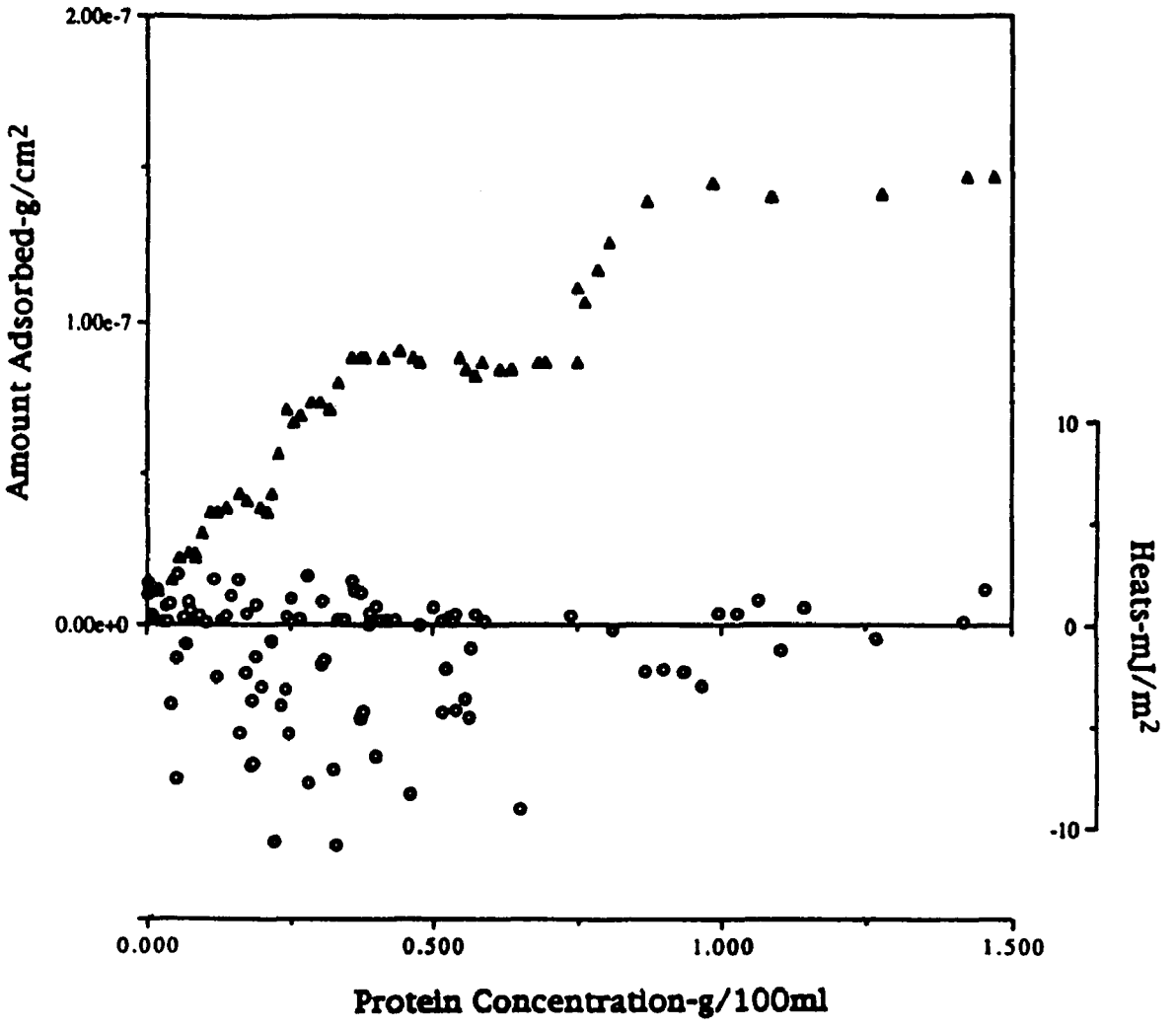

Fig. 26. Adsorption isotherm (▲) and microcalorimetric heats (o) for polystyrene at ionic strength of 0.002M from phosphate buffer.

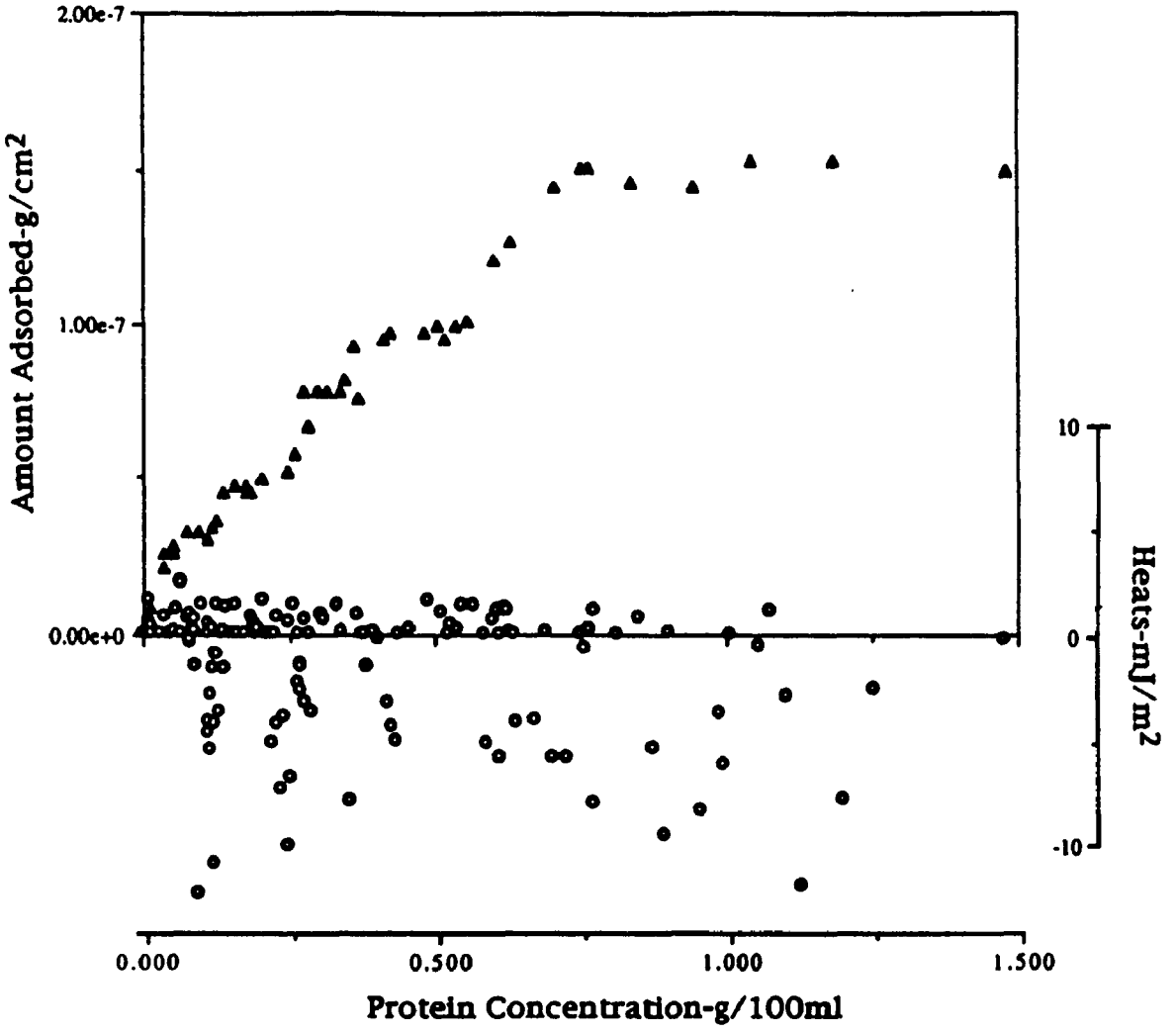

Fig. 27. Adsorption isotherm (▲) and microcalorimetric heats (o) for styrene/butyl methacrylate at ionic strength of 0.002M from phosphate buffer.

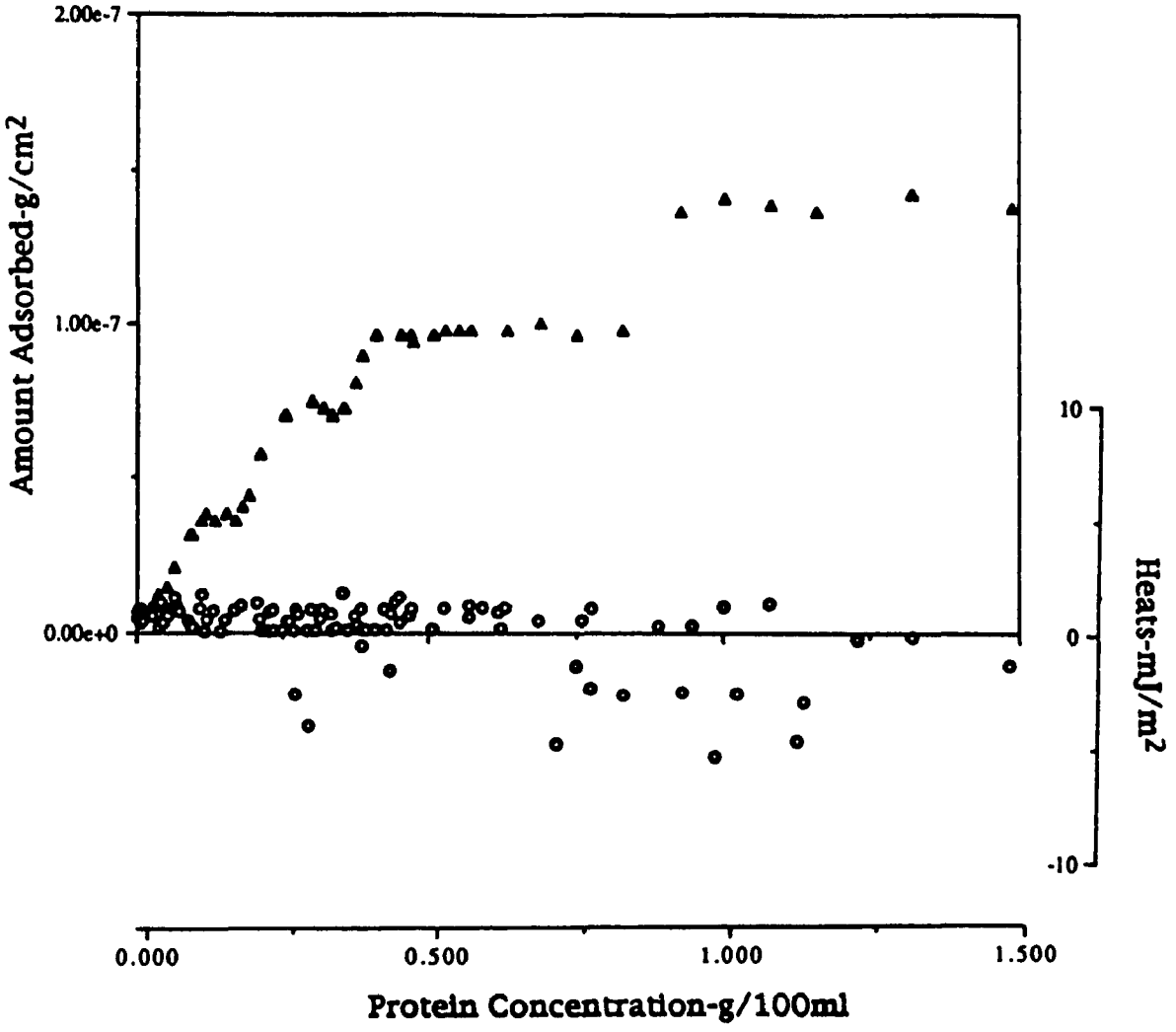

Fig. 28. Adsorption isotherm (▲) and microcalorimetric heats (o) for styrene/allyl alcohol at ionic strength of 0.002M from phosphate buffer.

The shorter plateaus in Figs. 26-28 are a reflection of the lower ionic strength, but a connection is not clear. Ionic strength has been reported to both increase[45] and decrease[44] adsorption by its screening action, and by co-adsorbing onto the surface along with protein[100].

Conclusions regarding the effect of interfacial energy on adsorption are difficult to make due to the problems of accurately ranking materials of similar interfacial properties. If endothermic discontinuities represent latent heats, their absence in the case of poly(co-styrene-allyl alcohol) indicates that transitions on that material involve relatively little structural rearrangement. This interpretation implies that adsorption by poly(co-styrene-allyl alcohol) results in conformations that are quite different than does adsorption by polystyrene or by poly(co-styrene-butyl methacrylate).

Changes in peak height ratios of amide I and II bands, Fig. 22, indicate conformational changes upon adsorption and show an increasing trend in the order; polystyrene : poly(co-styrene-butyl methacrylate) : poly(co-styrene-allyl alcohol). Since the ratios reflect α-helix content only, the trend does not indicate with which material structural changes were greatest.

Calorimetric results correlate somewhat with sample interfacial properties and FTIR peak ratios. Polystyrene was estimated by both methods to have the highest interfacial energy, and poly(co-styrene-allyl alcohol) by one method to have the lowest.

No differences in binding affinities, or initial slopes of isotherms, were found. A slightly smaller adsorbed amount at final plateau concentrations for poly(co-styrene-allyl alcohol) substrate in 0.002M buffer was noted.

While the effect on adsorption by multiple forms of lysozyme is not known, protein heterogeneity might account for the large number of plateaus.

Albumin, for which isotherms with several plateaus have been reported, has been found to show multiple forms upon gel filtration on Sephadex G-200[107].

CHAPTER V

SUMMARY

Lysozyme, a well-characterized globular enzyme, was purified by cation-exchange chromatography. Purity of the three major fractions retained for use in this work was verified by gel electrophoresis. Water content of the lyophilized protein was determined to be 8.90%.

High surface area substrates of polystyrene, poly(co-styrene-butyl methacrylate) and poly(co-styrene-allyl alcohol) for microcalorimetry were prepared by allowing adsorption of polymer from solution onto fumed silica. Polymer layer thickness was estimated in the case of polystyrene to be about 50 Angstroms. Sample surface areas, as measured by the BET method, were determined to be 71, 93 and 85 m^2/g, respectively. Flat polymer samples for static and dynamic contact angles were prepared by allowing adsorption from solution by oxide-covered silicon wafers. The minimum thickness of polystyrene required to mask silicon oxide properties was determined to be 40 Angstroms.

Polymer/water interfacial energies were estimated from the published surface tension of water and from surface tensions of each polymer determined using the pendant drop method. Estimates of the work of adhesion at the interface were made using a harmonic mean equation. Polar and

dispersion components of the surface energy of each polymer for use in the harmonic mean equation were determined using two methods. First, contact angles of two liquids on each polymer along with the harmonic mean equation in combination with Young's equation allowed the estimation of the component energies by simultaneous solution of two equations. Second, the dispersion component was estimated for each polymer from the contact angle of methylene iodide, a liquid whose interactions are primarily dispersion, and a geometric mean equation. The polar component was then determined as the difference from the surface energy as found from pendant drop results. Both methods predicted the polystyrene/water interfacial energy to be highest of the three, and one method predicted the poly(co-styrene-allyl alcohol) energy to be lowest.

The Wilhelmy plate study verified the time-dependent nature of substrate/water interfacial properties. It was determined that 48 hours of water contact time was sufficient for sample equilibration.

Peak height ratios of amide I and II bands in the infrared spectra of polymer/lysozyme complexes showed considerable change compared to the ratio of the bands of bulk lysozyme, strongly suggesting structural rearrangement upon adsorption. Peak height ratios of adsorbed lysozyme increased in the order; polystyrene < poly(co-styrene-butyl methacrylate) < poly(co-styrene-allyl alcohol), indicating a dependence of structural rearrangement on substrate. Since the ratio is a reflection of α-helix content only, the trend does not indicate on which material structural changes are greatest.

The amount of lysozyme adsorbed by each substrate was monitored by a depletion method and ultraviolet spectroscopy. Distinct step patterns were found in each adsorption isotherm. Plateau concentrations of lysozyme

ranged from 18% to 85% if the molecule adsorbed "side-on" without spreading, suggesting that the plateaus do not represent multiple layers. The shape of the adsorption isotherms is consistent with Levine's model which proposes the occurrence of multiple protein conformational states and the coexistence of two phases during transition.

Integral heats of adsorption of lysozyme for sample polymers were obtained in the monolayer and submonolayer regions using a microcalorimeter. In the cases of polystyrene and poly(co-styrene-butyl methacrylate), endothermic heats occurred at rises between plateaus. Endothermic heats were largely undetectable in the case of poly(co-styrene-allyl alcohol). The magnitudes of endothermic heats in the cases of polystyrene and poly(co-styrene-butyl methacrylate), 7-12 mJ/m^2, agree well with the 7 mJ/m^2 found by Norde and Lyklema to be the contribution from structural rearrangement to the integral heat of adsorption of ribonuclease, a globular protein with structural stability similar to that of lysozyme. This result, along with the absence of similar heats along the initial ascending part of the adsorption isotherms, suggests that the discontinuities are associated with transitions between lysozyme conformational states, and are probably latent heats. The absence of detectable heats along plateaus in the presence of spectroscopic evidence of structural rearrangement suggests the presence of other heat-generating subprocesses, such as ion transfer.

Endothermic heats during spontaneous adsorption indicate a gain in entropy, most likely associated with structural rearrangement. The absence of such heats in the case of poly(co-styrene-allyl alcohol) suggests that transitions on that surface occur with smaller structural change than do transitions on polystyrene and on poly(co-styrene-butyl methacrylate). In turn, the conformational state upon adsorption at any point by poly(co-

styrene-allyl alcohol) is likely quite different from that upon adsorption by the other two materials. Given the trend in amide band peak height ratios, structural changes upon adsorption by polystyrene and by poly(co-styrene-butyl methacrylate) may be greater than are those by poly(co-styrene-allyl alcohol).

It was not possible to adequately determine the effect of interfacial energy on adsorption. The range of interfacial properties of the materials chosen was narrow, and the methods used to estimate them did not give consistent results. Both methods predicted polystyrene to have the highest interfacial energy of the three, and one method predicted poly(co-styrene-allyl alcohol) to have the lowest.

CHAPTER VI

CONCLUSIONS

(1) Polystyrene, poly(co-styrene-butyl methacrylate) and poly(co-styrene-allyl alcohol) show time-dependent changes in surface properties upon contact with water.

(2) Lysozyme undergoes structural rearrangement upon adsorption by the above three polymers. The extent of rearrangement upon adsorption depends on the substrate.

(3) Step patterns in the adsorption isotherms of lysozyme on polystyrene, poly(co-styrene-butyl methacrylate) and poly(co-styrene-allyl alcohol) represent multiple surface conformational states of lysozyme.

(4) Endothermic discontinuities occurring at rises between plateaus in adsorption isotherms of lysozyme on the above three polymers are probably latent heats associated with transitions between two conformational states of lysozyme.

(5) Greater conformational changes in lysozyme possibly occur upon adsorption by polystyrene and poly(co-styrene-butyl methacrylate) than bypoly(co-styrene-allyl alcohol).

APPENDICES

APPENDIX A

PROCEDURE - GEL ELECTROPHORESIS

Reagent preparation: Deionized water was used throughout. Solutions were adjusted for pH at 25°C.

A) Acrylamide solution: 48g acrylamide and 1.5g N,N'-methylene-bis-acrylamide were dissolved in water to a final volume of 100ml.

B) Gel buffer: 36.34g Trizma base and 0.30g Sodium dodecylsulfate were dissolved in 60ml water. pH was adjusted to 4.85 with concentrated HCl. Volume was adjusted to 100ml with water.

C) SDS stock solution, 20%: 10.0g sodium lauryl sulfate was dissolved in 50ml water.

D) Tris · HCl, 1M, pH 6.8: 12.1g Trizma base was dissolved in 80ml water. pH was adjusted to 6.8 with concentrated HCl. Volume was adjusted to 100ml with water.

E) Sample buffer: The following were combined: 4.0ml 20% SDS (Solution C)
2.4 ml glycerol
0.4ml 2-mercaptoethanol
2.0ml Brilliant Blue G
1.0ml Tris · HCl, 1M, pH 6.8 (Sol. D)
Volume was adjusted to 20.0 ml with water.

F) Ammonium persulfate solution: 100mg ammonium persulfate was dissolved in 1.0ml of water.

G) Anode buffer: 121.1g Trizma base was dissolved in 1.0 liter of water. pH was adjusted to 8.9 with concentrated HCl. Volume was adjusted to 5 liters with water.

H) Cathode buffer: 12.11g Trizma base, 17.92g Tricine and 1.0g sodium lauryl sulfate were dissolved in a liter of water.

I) Fixative solution: 50ml methanol and 10ml glacial acetic acid were combined, and volume was adjusted to 100ml with water.

J) Staining solution: 50mg Brilliant Blue G was dissolved in 200ml glacial acetic acid. The solution was stirred for 30 minutes and filtered.

K) Destaining solution: 100ml glacial acetic acid was combined with 900ml of water.

Sample Preparation: Samples were prepared at a concentration of 1mg/ml in sample buffer (Solution E). Molecular weight markers were prepared by reconstituting vial contents with 2.2ml sample buffer (Solution D). All samples and molecular weight markers solution were incubated for 30 minutes at 40°C and allowed to cool to room temperature.

Preparation of electrophoresis gels:

	Stacking Gel Sol. (1-2cm)	Spacer Gel Sol. (2-3cm)	Separating Gel Sol. (10cm)
Acrylamide sol. (Solution A)	1.0ml	6.1ml	10.0ml
Gel buffer (Solution B)	3.1ml	10.0ml	10.0ml
Glycerol	--	--	3.2ml
Water	8.4ml	13.9ml	6.8ml

1) Solutions were pipetted as indicated above, and then deaerated.

2) Preparation of separating gel solution was completed by adding 0.1ml ammonium persulfate (Solution F) and 0.01 ml TEMED and mixing.

3) Preparation of spacer gel solution was completed by adding 0.1ml ammonium persulfate (Solution F) and 0.01ml TEMED and mixing.

4) Separating gel solution was poured to a height of 10cm and then overlayed with spacer gel solution to 12cm. The spacer gel was overlayed with water.

5) After separating and spacer gels were polymerized, water overlay was removed. 0.1ml ammonium persulfate (Solution F) and 0.01ml TEMED were added to 12.5ml of stacking gel solution, mixed poured onto the spacer gel.

6) The well-forming comb was inserted into the stacking gel.

7) After the gel was set, it was allowed to equilibrate overnight at 4°C.

Electrophoresis:

1) The wells were rinsed with water, then with cathode buffer (Solution H).

2) 10μl of molecular weight markers solution were underlaid per well. Samples (5-10μg) were loaded.

3) A constant current of 20mA was applied for 1 hour, allowing the samples to completely enter the stacking gel. The current was then increased to 30mA and maintained throughout the remainder of the run, typically 16 hours.

4) Current was applied until the marker dye was within 1cm of the anodic end of the gel.

5) The gel was removed and immersed in the fixative solution (Solution I) for 60 minutes.

6) The gel was transferred to staining solution (Solution J) for 2 hours.

7) The gel was transferred to destaining solution (Solution K) for 2 hours, renewing the solution every 30 minutes.

8) The gel was photographed.

APPENDIX B

COMPONENTS OF SURFACE ENERGY AND INTERFACIAL ENERGIES OF SAMPLE POLYMERS

Polar and dispersion components of sample polymers: The components were estimated from contact angles of water and methylene iodide on the sample polymers and the following equation[87]:

$$\gamma_{12} = \gamma_1 + \gamma_2 - \frac{4\gamma_1^d \gamma_2^d}{\gamma_1^d + \gamma_2^d} - \frac{4\gamma_1^p \gamma_2^p}{\gamma_1^p + \gamma_2^p} \tag{1}$$

which was rearranged to two simultaneous equations by combination with Young's equation

$$\gamma_{lg} \cos\theta = \gamma_{sg} - \gamma_{sl} \tag{2}$$

to give

$$1 + \cos\theta = \frac{1}{\gamma_{water}} \left[\frac{4\gamma_{polymer}^d \gamma_{water}^d}{\gamma_{polymer}^d + \gamma_{water}^d} + \frac{4\gamma_{polymer}^p \gamma_{water}^p}{\gamma_{polymer}^p + \gamma_{water}^p} \right] \tag{3}$$

$$1 + \cos\theta = \frac{1}{\gamma_{MeI}} \left[\frac{4\gamma_{polymer}^d \gamma_{MeI}^d}{\gamma_{polymer}^d + \gamma_{MeI}^d} + \frac{4\gamma_{polymer}^p \gamma_{MeI}^p}{\gamma_{polymer}^p + \gamma_{MeI}^p} \right] . \tag{4}$$

The value of the surface tension of water is from reference [108]. The polar and dispersion components of water are those used by Fowkes, who estimated the dispersion component from measurements of the interfacial tension of water against a series of nonpolar liquids of known surface tensions, and applying a geometric mean approximation[55].

The surface tension and components of methylene iodide are those used by Wu, who estimated the component tensions from known surface and interfacial tensions of water and methylene iodide, and the harmonic mean approximation[87].

Interfacial energies: Interfacial energies were estimated from equation (1), where γ_1 is the surface energy of the polymer as determined by the pendant drop method, γ_2 is the surface tension of water, and the $\gamma_{polymer,water}^{d,p}$ terms are the polar and dispersion components of the polymer and of water.

APPENDIX C

TABULATED DATA

Figure 10:

Polystyrene:		Styrene/ butyl methacrylate:		Styrene/ allyl alcohol	
Conc. (g/100ml)	Amount adsorbed (g/g silica)	Conc. (g/100ml)	Amount adsorbed (g/g silica)	Conc. (g/100ml)	Amount adsorbed (g/g silica)
0.0011	0.060	0.0031	0.095	0.030	0.30
0.010	0.34	0.0088	0.31	0.084	0.37
0.050	0.57	0.021	0.39	0.30	0.40
0.50	0.64	0.042	0.39	0.64	0.45
1.0	0.66	0.38	0.45	1.0	0.58
1.5	0.65	1.0	0.51	1.5	0.60
2.5	0.72	1.5	0.56	2.0	0.73
3.3	0.73	2.0	0.61	2.5	0.74
4.0	0.75	2.9	0.70	3.0	0.85
		4.0	0.75	3.5	0.85
				4.0	0.89

Figure 12:

Water in octane		Octane in water	
Thickness (Angstroms)	Contact Angle (Degrees)	Thickness (Angstroms)	Contact Angle (Degrees)
0	16	0	155
4	75	24	90
7	95	27	63
9	94	35	40
10	103	37	37
12	103	39	25
13	106	45	16
24	104	48	25

31	108	50	22
34	108	54	27
37	108	59	16
40	109	63	29
92	108	96	27
		106	18

Figure 13:

Polystyrene:		Styrene/ butyl methacrylate:		Styrene/ allyl alcohol:	
Temp. °C	Surface Tension (dynes/cm)	Temp. °C	Surface Tension (dynes/cm)	Temp. °C	Surface Tension (dynes/cm)
132	0.973	108	0.966	70	0.954
147	0.965	122	0.954	75	0.954
162	0.945	133	0.945	80	0.954
175	0.935	147	0.937	85	0.951
				90	0.947
				95	0.947

Figure 14:

Polystyrene:		Styrene/ butyl methacrylate:		Styrene/ allyl alcohol:	
Temp. °C	Density (g/cm^3)	Temp. °C	Density (g/cm^3)	Temp. °C	Density (g/cm^3)
127.10	0.9995	110.96	0.9940	75.60	1.0475
138.60	0.9929	119.98	0.9881	86.35	1.0392
153.74	0.9816	130.16	0.9799	95.55	1.0331
168.73	0.9692	139.82	0.9713	108.02	1.0243
		149.46	0.9629		

Figure 16:

	Polystyrene:		Styrene/ butyl methacrylate:		Styrene/ allyl alcohol:	
Time (hours)	Advanc. angle	Reced. angle	Advanc. angle	Reced. angle	Advanc. angle	Reced. angle
0	98	75	95	72	94	30
0.33	95	67	94	67	88	16
0.75	94	71	94	68	86	22
1.5	93	70	92	68	85	25
3.0	91	66	90	65	83	27
5.0	90	60	89	60	82	26
7.0	91	57	88	51	82	25
8.0	91	55	88	51	83	23
19	87	48	87	44	81	29
23	87	49	85	42	79	29
29	87	48	84	42	76	26

Figure 17:

	Polystyrene:		Styrene/ butyl methacrylate:		Styrene/ allyl alcohol:	
Time (hours)	Advanc. angle	Reced. angle	Advanc. angle	Reced. angle	Advanc. angle	Reced. angle
0	91	65	96	53	98	48
0.16	91	65	93	53	94	47
0.50	91	65	92	52	93	47
1.0	91	64	92	52	92	49
2.0	90	61	91	50	91	48
3.25	90	60	92	48	92	45
5.16	90	58	92	47	92	42
6.16	90	56	91	45	92	41
7.50	90	55	91	45	91	40
8.50	89	55	90	43	90	40
9.50	89	54	90	42	89	38
10.5	90	53	90	42	89	37
21.5	90	47	90	38	90	35
32.0	90	46	89	37	88	31

Figure 19:

Polystyrene:

Conc. (g/100ml)	Amount (g/cm^2)
0.0072	4.3e-9
0.0191	8.7e-9
0.0284	1.3e-8
0.0434	1.7e-8
0.0692	2.8e-8
0.0792	3.3e-8
0.0888	3.3e-8
0.109	4.1e-8
0.118	4.8e-8
0.139	6.1e-8
0.153	7.4e-8
0.168	8.7e-8
0.198	8.7e-8
0.221	8.7e-8
0.237	8.9e-8
0.260	8.7e-8
0.279	9.1e-8
0.302	9.1e-8
0.321	9.1e-8
0.333	9.5e-8
0.354	1.1e-7
0.374	1.3e-7
0.437	1.3e-7
0.458	1.3e-7
0.470	1.4e-7
0.486	1.5e-7
0.491	1.5e-7
0.512	1.6e-7
0.528	1.8e-7
0.540	1.9e-7
0.570	1.8e-7
0.590	1.8e-7
0.624	1.8e-7
0.648	2.0e-7
0.662	2.0e-7
0.690	2.3e-7
0.702	2.4e-7
0.403	1.3e-7

Figure 20:

Styrene/ butyl methacrylate:

Conc. (g/100ml)	Amount (g/cm^2)
0.0165	6.5e-9
0.0302	1.1e-8
0.0440	1.9e-8
0.0536	2.2e-8
0.0647	2.4e-8
0.0749	2.6e-8
0.0798	2.8e-8
0.101	3.2e-8
0.117	3.7e-8
0.132	4.1e-8
0.148	4.7e-8
0.171	6.5e-8
0.185	6.7e-8
0.197	6.9e-8
0.224	6.9e-8
0.264	6.9e-8
0.282	8.2e-8
0.294	1.1e-7
0.318	1.1e-7
0.366	1.1e-7
0.404	1.0e-7
0.428	1.3e-7
0.446	1.7e-7
0.458	1.7e-7
0.458	1.9e-7
0.495	2.0e-7
0.512	2.0e-7
0.540	1.9e-7
0.566	1.9e-7
0.582	1.9e-7
0.624	1.9e-7
0.665	2.1e-7
0.699	2.2e-7
0.719	2.1e-7
0.761	2.1e-7

Figure 21:

Styrene/ allyl alcohol:

Conc. (g/100ml)	Amount (g/cm^2)
0.016	3.2e-9
0.046	1.7e-8
0.067	1.9e-8
0.095	2.6e-8
0.105	3.4e-8
0.140	4.5e-8
0.164	5.1e-8
0.197	6.2e-8
0.204	6.2e-8
0.239	8.7e-8
0.279	9.6e-8
0.318	9.2e-8
0.352	9.0e-8
0.387	9.1e-8
0.410	9.0e-8
0.422	1.0e-7
0.484	1.4e-7
0.510	1.4e-7
0.595	1.4e-7
0.620	1.4e-7
0.641	1.9e-7
0.657	1.9e-7
0.707	1.9e-7
0.723	1.9e-7

Figure 26:

Polystyrene:

Conc. (g/100ml)	Amount (g/cm^2)
0.011	2.8e-9
0.020	1.1e-8
0.043	1.5e-8
0.055	2.3e-8
0.072	2.4e-8
0.082	2.3e-8
0.083	2.4e-8
0.094	3.0e-8
0.109	3.7e-8
0.122	3.7e-8
0.138	3.9e-8
0.161	4.3e-8
0.174	4.1e-8
0.195	3.9e-8
0.210	3.7e-8
0.218	4.3e-8
0.228	5.6e-8
0.245	7.2e-8
0.254	6.7e-8
0.269	6.9e-8
0.287	7.4e-8
0.303	7.4e-8
0.317	7.2e-8
0.335	8.0e-8
0.356	8.9e-8
0.374	8.9e-8
0.381	8.9e-8
0.411	8.9e-8
0.438	9.1e-8
0.462	8.9e-8
0.474	8.7e-8
0.546	8.9e-8
0.558	8.5e-8
0.575	8.2e-8
0.587	8.7e-8
0.617	8.5e-8
0.635	8.5e-8
0.684	8.7e-8
0.693	8.7e-8
0.752	8.7e-8
0.752	1.1e-7
0.764	1.1e-7
0.785	1.2e-7
0.806	1.3e-7

Figure 27:

Styrene/ butyl methacrylate:

Conc. (g/100ml)	Amount (g/cm^2)
0.012	8.6e-9
0.036	2.2e-8
0.036	2.6e-8
0.051	2.6e-8
0.052	2.8e-8
0.076	3.2e-8
0.093	3.2e-8
0.109	3.0e-8
0.119	3.4e-8
0.124	3.7e-8
0.138	4.5e-8
0.156	4.7e-8
0.174	4.7e-8
0.176	4.5e-8
0.183	4.5e-8
0.204	5.0e-8
0.248	5.2e-8
0.258	5.8e-8
0.272	7.7e-8
0.281	6.7e-8
0.297	7.7e-8
0.312	7.7e-8
0.336	7.7e-8
0.345	8.2e-8
0.360	9.3e-8
0.369	7.5e-8
0.410	9.5e-8
0.423	9.7e-8
0.479	9.7e-8
0.503	9.9e-8
0.516	9.5e-8
0.536	9.9e-8
0.554	1.0e-7
0.600	1.2e-7
0.630	1.3e-7
0.705	1.4e-7
0.752	1.5e-7
0.761	1.5e-7
0.836	1.5e-7
0.941	1.4e-7
1.04	1.5e-7
1.18	1.5e-7
1.48	1.5e-7

Figure 28:

Styrene/ allyl alcohol:

Conc. (g/100ml)	Amount (g/cm^2)
0.012	6.4e-9
0.036	1.3e-8
0.050	1.5e-8
0.063	2.1e-8
0.090	3.2e-8
0.095	3.2e-8
0.108	3.6e-8
0.117	3.8e-8
0.134	3.6e-8
0.152	3.8e-8
0.170	3.6e-8
0.182	4.1e-8
0.191	4.5e-8
0.210	5.8e-8
0.254	7.0e-8
0.302	7.5e-8
0.320	7.3e-8
0.336	7.0e-8
0.354	7.3e-8
0.374	8.1e-8
0.387	9.0e-8
0.411	9.6e-8
0.453	9.6e-8
0.470	9.6e-8
0.474	9.4e-8
0.507	9.6e-8
0.528	9.8e-8
0.549	9.8e-8
0.570	9.8e-8
0.635	9.8e-8
0.689	1.0e-7
0.752	9.6e-8
0.828	9.8e-8
0.929	1.4e-7
1.00	1.4e-7
1.08	1.4e-7
1.16	1.4e-7
1.32	1.4e-7
1.49	1.4e-7

0.873	1.4e-7
0.986	1.5e-7
1.09	1.4e-7
1.28	1.4e-7
1.42	1.5e-7
1.47	1.5e-7

BIBLIOGRAPHY

1. P.N. Sawyer, B. Stanczewski and F.D. Mistry, Biologic and Synthetic Vascular Prostheses, eds. J.C. Stanley et al., Grune and Stratton, New York, (1982).

2. J.W. Pate and P.N. Sawyer, Surg., **34**, 491-500 (1953).

3. C.P. Sharma, Biomaterials, **2**, 57-59 (1981).

4. L. Vroman, Biomat. Med. Dev. Art. Org., **12**, 307-323 (1984).

5. R.E. Baier, J. Biomed. Mater. Res., **3**, 191-206 (1969).

6. R.C. Eberhart, H.H. Huo and K. Nelson, MRS Bulletin, vol. XVI, no. 9, 50-54 (1991).

7. E. Ruckenstein and S.V. Gourisankar, Biomaterials, **7**, 403-422 (1986).

8. L. Weiss, The Cell Periphery, Metastasis and Other Contact Phenomena, North Holland, Amsterdam, pp. 248-252 (1967).

9. F. MacRitchie, Adv. Protein Chem., **32**, 283-326 (1978).

10. J. Lyklema, Affinity Chromatography, 11-27, ed. T.C.J. Gribnau, Elsevier, Amsterdam, (1982).

11. B.H.J. Hofstee and N.F. Otillio, J. Chromatog., **159**, 57-69 (1978).

12. Y. Kobayaski and S. Aomine, Soil Science and Plant Nutrition, **13**, 189 (1967).

13. J.L. Brash and D.J. Lyman, Chemistry of Biosurfaces, vol. 1, pp. 172-232, Dekker, New York, (1971).

14. D.F. Chessman and J.T. Davies, Adv. Protein Chem., **9**, 439-506 (1954).

15. P.A. Cuypers, W.T. Hermens and H.C. Hemker, Ann. New York Acad. Sci., **283**, 77-85 (1977).

16. U. Jonsson, B. Ivarsson, I. Lundstrom and L. Berghem, J. Colloid Interface Sci., **90**, 148-163 (1982).

17. W. Norde and J. Lyklema, J. Colloid Interface Sci., **66**, 257-265 (1978).

18. P.G. Koutsoukos, W. Norde and J. Lyklema, J. Colloid Interface Sci., **95**, 385-395 (1983).

19. T.P. Burghardt and D. Axelrod, Biochemistry, **22**, 979-985 (1983).

20. C.R. McMillin and A.G. Walton, J. Colloid Interface Sci., **48**, 345-349 (1974).

21. B. Benko, S. Vukk-Pavlovic, G. Dezelic and S. Maricic, J. Colloid Interface Sci., **52**, 444-451 (1975).

22. M.E. Soderquist and A.G. Walton, J. Colloid Interace Sci., **75**, 386-397 (1980).

23. F.E. Filisko, D. Malladi and S. Barenberg, Biomaterials, **7**, 348-353 (1986).

24. E. Nyilas, T.H. Chiu, and G.A. Herzlinger, Trans. Am. Soc. Art. Int. Org., **20**, 480-490 (1974).

25. E. Nyilas, T.H. Chiu, and D.M. Lederman, Colloid and Interface Science, vol. 5, Academic Press, New York, pp. 77-89 (1976).

26. T.H. Chir, E. Nyilas, and D.M. Lederman, Trans. Am. Soc. Art. Int. Org., **22**, 498-513 (1976).

27. A. Takahashi and M. Kawaguchi, Adv. in Polymers Sci., **46**, 3-65 (1982).

28. W. Norde, Adv. in Coll. and Interface Sci., **25**, 290-294 (1986).

29. B.D. Fair and A.M. Jamison, J. Colloid Interface Sci., **77**, 525-534 (1980).

30. V. Hlady and H. Furedi-Milhofer, J. Colloid Interface Sci., **69**, 460 (1979).

31. H.B. Bull, Biochim. Biophys. Acta, **19**, 464 (1956).

32. W. Norde and J. Lyklema, J. Colloid Interface Sci., **66**, 257 (1978).

33. F. MacRitchie, J. Colloid Interface Sci., **38**, 484 (1972), (in W. Norde, Adv. in Coll. and Interface Sci., **25**, 290-294 (1986)).

34. G. Penners, Z. Priel and A. Silberberg, J. Colloid Interface Sci., **80**, 437-444 (1982).

35. J.L. Brash and V.J. Davidson, Thrombosis Research, **9**, 259-269 (1976).

36. W.J. Dillman and I.F. Miller, J. Colloid Interface Sci., **44**, 221 (1973), (in W. Norde, Adv. in Coll. and Interface Sci., **25**, 290-294 (1986)).

37. F. Grinnell and M.K. Feld, J. Biomed. Mater. Res., **15**, 363-381 (1981).

38. K.S. Birdi, J. Colloid Interface Sci., **43**, 545 (1973), (in W. Norde, Adv. in Coll. and Interface Sci., **25**, 290-294 (1986)).

39. W. Norde and J. Lyklema, J. Colloid Interface Sci., **66**, 295-302 (1978).

40. W. Norde and J. Lyklema, J. Colloid Interface Sci., **66**, 266-276 (1978).

41. W. Norde and J. Lyklema, J. Colloid Interface Sci., **66**, 277-284 (1978).

42. W. Norde and J. Lyklema, J. Colloid Interface Sci., **66**, 285-294 (1978).

43. P. Bagchi and S.M. Birnbaum, J. Colloid Interface Sci., **83**, 460-478 (1981).

44. P.G. Koutsoukos, C.A. Mumme-Young, W. Norde and J. Lyklema, Colloids and Surfaces, **5**, 93-104 (1982).

45. T. Mizutani, J. Colloid Interface Sci., **82**, 162-166 (1981).

46. P.A. Cuypers, W.T. Hermens and H.C. Hemker, Anal. Biochem., **84**, 56-67 (1978).

47. M. Korn and E. Killman, J. Colloid Interface Sci., **76**, 119-131 (1980).

48. F.J. Holly and M.F. Refojo, J. Biomed. Mater. Res., **9**, 315-326 (1975).

49. C.S.P. Sung and C.B. Hu, J. Biomed. Mater. Res., **13**, 45-55 (1979).

50. J. Tse and A.W. Adamson, J. Colloid Interface Sci., **72**, 515-523 (1979).

51. R.J. Good and E.D. Kotsidas, J. Colloid Interface Sci., **66**, 360-362 (1978).

52. J.D. Andrade, D.E. Gregonis and L.M. Smith, Physicochemical Aspects of Polymer Surfaces, vol. 2, Plenum Press, New York (1983).

53. H. Yasuda, A.K. Sharma, and T. Yasuda, J. Polym. Sci. Poly. Phys. Ed., **19**, 1285-1291 (1981).

54. L.Smith, C. Doyle, D.E. Gregonis, and J.D. Andrade, Physicochemical Aspects of Polymer Surfaces, ed. K. Mittal, Plenum Press, New York, p.911-922, (1983).

55. F.M. Fowkes, Industrial and Engineering Chemistry, **56**, 40-52 (1964).

56. J.D. Andrade, S.M. Ma, R.N. King, D.E. Gregonis, J. Colloid Interface Sci., **72**, 488-494 (1979).

57. S. Wu, J. Adhesion, **5**, 39-55 (1973).

58. Y.C. Ko, B.D. Ratner, and A.S. Hoffman, J. Colloid Interface Sci., **82**, 25-37 (1981).

59. B.D. Ratner, A.S. Hoffman, S.R. Hanson, L.A. Harkar, J.D. Whiffen, J. Polym. Sci., Polym. Symp., No. 66, 363 (1979).

60. E. Brynda, N.S. Cepalova and M. Stol, J. Biomed. Mater. Res., **18**, 685-693 (1984).

61. A. Baszkin and D.J. Lyman, J. Biomed. Mater. Res., **14**, 393-403 (1980).

62. R.E. Baier, Adhesion in Biological Systems, ed. R.S. Manly, Academic Press, New York, p. 15 (1970).

63. I.H. Segel, Biochemical Calculations, 2nd ed., John Wiley & Sons, New York, p. 57, (1976).

64. V.P. Saxena and D.B. Wetlaufer, Biochemistry, **9**, 5015-5022 (1970).

65. Sigma Technical Bulletin no. MWM-100, p. 1-7, Septemper 1990.

66. Sprouse Collection of Infrared Spectra, Book 1:Polymers, ed. Diana L. Hanson, Sprouse Scientific Systems, Inc., p. 162, (1987).

67. Desk Book of Infrared Spectra, 2nd ed., ed., Clara D. Craver, Coblentz Society, p. 423, (1986).

68. J.S. Trent, J.I. Scheinbeim, P.R. Couchman, Macromolecules, **16**, 589-598 (1983).

69. J.D. Andrade, Surface and Interfacial Aspects of Biomedical Polymers, vol. 1, p. 262, ed. J.D. Andrade, Plenum Press, New York, (1985).

70. S. Wu, J. Colloid Interface Sci., **31**, 153-161 (1969).

71. J.M. Andreas, E.A. Hauser, W.B. Tucker, J. Phys. Chem., **42**, 1001 (1938).

72. H.A. Skinner, Biochemical Microcalorimetry, ed. H.D. Brown, Academic Press, New York, p. 7, (1969).

73. O. Stevens and G.. Bergstrom, Proc. Soc. Exp. Bio. Med., **124**, 187 (1967).

74. P. Jolles, The Enzymes, ed. P.D. Boyer, Academic Press, New York, vol. 4, p. 431 (1960).

75. D. Givol, F. DeLorenzo, R.F. Goldberger, and C.B. Anfinsen, Proc. Nat. Acad. Sci., **153**, 676 (1965).

76. E.M. Prager and A.C. Wilson, J. Biol. Chem., **246**, 523 (1971).

77. J. Jolles, E. van Leemputten, A. Mouton, and P. Jolles, Biochim. Biophys., Acta, 257, **497** (1972).

78. R.S. McDonald, J. Phys. Chem., **62**, 1168-1178 (1958).

79. M.A. Cohen-Stuart, H.M. Scheutjens and G.J. Fleer, J. of Polymer Sci., **18**, 559 (1980).

80. Scientific Polymer Products, personal communication, January 4, 1993.

81. Z. Kessaissia, E. Papirer, J.P. Donnet, J. Colloid Interface Sci., **82**, 526-533 (1981).

82. H. Schonhorn, F.W. Ryan, J. Phys. Chem., **70**, 3811 (1966).

83. R.J. Roe, J. Phys. Chem., **69**, 2809 (1965).

84. J.D. Andrade, Medical Instrumentation, **7**, 110 (1973).

85. Polymer Handbook, 3rd ed., ed. J. Brandrup and E.H. Immergut, Wiley-Interscience, p. V-82, New York, (1989).

86. D.K. Owens and R.C. Wendt, J. of Applied Polymer Sci., **13**, 1741 (1969).

87. S. Wu, Recent Adv. Adhes., Proc. Am. Chem. Soc. Symp., ed. L.H. Lee, p. 45-63, (1971).

88. W.A. Zisman, Contact Angle, Wettability, and Adhesion, Adv. in Chem. Series, 43, p. 1, Washington (1964).

89. E.G. Shafrin and W.A. Zisman, Upper Limits for the Contact Angles of Liquids on Solids, N.R.L. Report 5985 (1963).

90. S. Wu, J. of Phys. Chem., **74**, 632-638 (1970).

91. R.J. Roe, J. of Phys. Chem., **72**, 2013-2017 (1968).

92. C.A. Girifalco and R.J. Good, J. Phys. Chem., **61**, 904 (1957).

93. J.D. Andrade, Surface and Interfacial Aspects of Biomedical Polymers, vol. 1, p. 337, ed. J.D. Andrade, Plenum Press, New York, (1985).

94. G. Castellan, Physical Chemistry, 3rd ed., p. 418, (1983).

95. R.E. Johnson, Jr. and R.H. Dettre, Surface and Colloid Science, vol. 2, p. 109, Wiley-Interscience, New York, (1969).

96. W. Norde and J. Lyklema, J. Biomater. Sci., Polym. Ed., 2(3), 183-202 (1991).

97. C.N. Pace, CRC Crit. Rev. Biochem., 3, 1 (1975).

98. J.D. Andrade, Surface and Interfacial Aspects of Biomedical Polymers, vol. 2, p. 26, Plenum Press, New York, (1985).

99. G.E. Schulz and R.H. Schirmer, Principles of Protein Structure, Springer-Verlaz, New York (1979).

100. G.J. Fleer and J. Lyklema, Makromol. Chem. Macromol. Symp., **17**, 39 (1988).

101. W. Norde and J. Lyklema, J. Colloid Interface Sci., 71, 350 (1979).

102. C.R. Cantor and P.R. Schimmel, Biophysical Chemistry, W.H. Freeman and Co., New York, pp. 297,609, (1980).

103. P.L. Privalov, Advanc. Protein Chem., **33**, 167 (1979).

104. Handbook of Biochemistry and Molecular Biology, 3rd ed., CRC Press, Cleveland, p. 210, (1977).

105. C.R. Cantor and P.R. Schimmel, Biophysical Chmistry, W.H. Freeman and Co., New York p. 468, (1980).

106. S.N. Levine, J. Biomed. Mater. Res., **3**, 83 (1969).

107. H. Olesen and P.O. Pederson, Acta Chem. Scand., **22**, 1386-1394 (1968).

108. CRC Handbook of Chemistry and Physics, 71st. ed., ed. D.R. Lide, Boca Raton, p. 6-8, (1990-1991).